Universidad de Cantabria
Departamento de Física Moderna

CSIC - Universidad de Cantabria
Instituto de Física de Cantabria

Una visión multifrecuencia de Núcleos de Galaxias Activas

Memoria presentada por el Licenciado

Ignacio Ordovás Pascual

para optar al título de Doctor en Ciencia y Tecnología

2018

Declaración de Autoría

Silvia Mateos Ibáñez, Doctora en Ciencias Físicas y Profesora Contratada Doctora de la Universidad de Cantabria,

y

Francisco Jesús Carrera Troyano, Doctor en Ciencias Físicas y Catedrático de la Universidad de Cantabria,

CERTIFICAN que la presente memoria

Una visión multifrecuencia de Núcleos de Galaxias Activas

ha sido realizada por **Ignacio Ordovás Pascual** bajo nuestra dirección.
Consideramos que esta memoria contiene aportaciones suficientes para construir la tesis Doctoral del interesado.

En Santander, a 11 de Septiembre de 2058

Silvia Mateos Ibáñez

Francisco Jesús Carrera Troyano

Ph'nglui mglw'nafh Cthulhu R'lyeh wgah'nagl fhtagn...

Agradecimientos

Déjame que pose para ti eres tú mi artista preferida déjame tenerte junto a mí prometo estarte agradecido prometo estarte agradecido. Si fuera yo capaz de conseguir tenerte alguna vez entretenida hacerte por lo menos sonreir prometo estarte agradecido prometo estarte agradecido.

No te lo pienses más baja la guardia y mira atrás nadie te va a alcanzar no tienes rival no tienes rival.

Me paso el tiempo viéndote venir y pasas a mi lado distraída si dejas que camine tras de ti prometo estarte agradecido prometo estarte agradecido.

Te tengo tantas cosas que decir y tú como si no fuera contigo la historia se repite y aún así prometo estarte agradecido prometo estarte agradecido.

No te lo pienses más baja la guardia y mira atrás nadie te va a alcanzar no tienes rival no tienes rival.

No te lo pienses más baja la guardia y mira atrás nadie te va a alcanzar no tienes rival no tienes rival.

Déjame que pose para ti eres tú mi artista preferida déjame tenerte junto a mí prometo estarte agradecido prometo estarte agradecido prometo estarte agradecido.

Resumen de la tesis en castellano

Objetivos de la Investigación

Relleno.

Planteamiento y metodología

Relleno.

Aportaciones originales

Relleno.

Conclusiones

Relleno.

Futuras líneas de investigación

Relleno.

Universidad de Cantabria
Departamento de Física Moderna

CSIC - Universidad de Cantabria
Instituto de Física de Cantabria

A multifrequency view of Active Galactic Nuclei

A dissertation submitted in partial fulfillment of the requirements
for the degree of Doctor in Science and Technology

by

Ignacio Ordovás Pascual

“I am your father.”

Lord Voldemort
(John Ronald Reuel Tolkien, Game of Thrones)

“The problem with quotes found on internet
is that they are often not true.”

Abraham Lincoln

Summary

Summary in english.

Contents

List of Figures

List of Tables

Chapter 1

Introduction

During the 18th and 19th centuries, it was not clear that some of the 'nebulas' seen in the sky were part of our galaxy, or they were 'islands-universes' compound by stars (Kant 1755). Since the discovery in 1924 of a Cepheid variable star in M31 (Hubble 1929), it became clear that some of them were extragalactic objects, or more precisely, they were galaxies like the Milky way. Using spectroscopic analysis, soon it became clear as well that some of the galaxies showed emission lines of highly ionized elements in the nuclei (Seyfert 1943) that cannot be explained just by the emission mechanisms of the stars, and so this emission is originated by a completely different phenomena. In some of this galaxies, this non stellar radiation completely outshines the galaxy starlight. This objects are called 'Active Galactic Nuclei' (AGN).

Nowadays, it is widely accepted that the origin of this emission is due to supermassive black holes (SMBH) of $>10^6$ $M_\odot$ in the centre of the active galaxy, whose immense gravitational potential is converted to emission due to very different mechanisms associated to the black hole, such as accretion of matter into the SMBH, incandescence or scattering of charged particles, among others (see Sec. 1.2 for a more detailed explanation). The reasons to accept that the SMBH are the objects responsible of this highly energetic phenomena are various. The emission of normal or quiescent galaxies is produced almost entirely by stars, and its emission is mainly constrained between UV and IR light. Meanwhile, AGN show emission across all the electromagnetic spectrum, from the gamma rays to radio energies. This means that active galaxies emits in over twenty orders of magnitude in frequency. The luminosity of the AGN ranges from bolometric luminosities of 10^{40} erg/s, comparable to the emission of quiescent galaxies ($L_{bol} < 10^{42}$ erg/s), to luminosities of 10^{48} erg/s. The active nuclei emission frequently outshines the host galaxy starlight due to this high luminosities. Depending on the energy band observed, AGN show strong time variability of years (optical/IR), days (UV) or minutes (X-rays). The time variability measurements of the AGN emission leaves not doubt that it is originated in a compact region of the order of miliparsecs. Taking together the high luminosity of the nuclei

emission and the compact region where they are originated, it is implied that AGN are objects with tremendous energy densities, only explainable by accretion into the SMBH in the core of the galaxy.

There are evidences of that almost every galaxy harbors a SMBH in the nuclei with a mass in the range of millions to billions of solar masses (Magorrian *et al.* 1998), but as the one in the Milky Way (10^6 $M_\odot$), not all of them are active. The host galaxy has a tight relation with its SMBH in the core of the galaxy. The M_{SMBH}/σ, M_{SMBH}/M_{Host}, M_{SMBH}/L_{host} plots show an evidence that both quantities are very related. It has been found that there is a coevolution of the black hole and the galaxy, so AGN are considered a stage in galactic evolution that can be created by accretion or galaxy mergers. The power of the winds of the AGN stops the star formation, as this feedback crosses all the galaxy (Fabian 2012). This means that the growth of the AGN is linked with the galaxy evolution (Kormendy and Ho 2013).

As active galaxies are the most luminous and long lived objects in the Universe, they are visible at a large range of distances. In addition, the most distant AGN to the date is at z=7.085 (Mortlock *et al.* 2011), when the universe was only about a 10% of its actual age. This also means that this object is the one closest objects in time to the Big Bang. The study of AGN therefore is a key to understand the evolution of the cosmos since the universe was very young.

The Cosmic X-ray Background (CXRB) spectrum is the composition of the total AGN emission. From the analysis of the power law index of this spectrum, it is clear that not all of the AGNs are unobscured. The power law is harder ($\Gamma_{CXRB} \simeq 1.4$ at E<10 keV) than an unobscured AGN ($\Gamma_{AGN} \simeq 1.9$), and X-ray absorption have more effect at lower energies. In order to match models with the observations, we must introduce a fraction of absorbed AGN and highly absorbed AGN whose extinction is Compton thick ($N_H > 10^{24} cm^{-2}$). The CXRB, using this assumption, is explained with a majority of absorbed AGN ,but to the date, this fraction of obscured sources is still unclear (Setti and Woltjer 1989, Comastri *et al.* 1995). The extinction of these sources plays a major role in understanding the intrinsic properties of AGN.

All of this facts are pieces of evidences of the big importance of the study of AGN. In this thesis we work on understanding the environment of the AGN through its emission properties and the optical extinction and X-ray absorption of these objects. This is an important aspect of AGN, as there are some open questions to the date that challenges the Unified Model of AGN (see Sec. 1.1).

1.1 Unified Model of AGN

There is a great variety of AGN with different observational properties whose power is originated by the same mechanism, that is the accretion to the SMBH, so an Unified Model of AGN was proposed to explain this diversity (Antonucci 1993, Urry and Padovani 1995). In this model, the observed differences between each class of AGN is dependent on the orientation. The Unified Model, schematically represented in Fig. 1.1, have the following components:

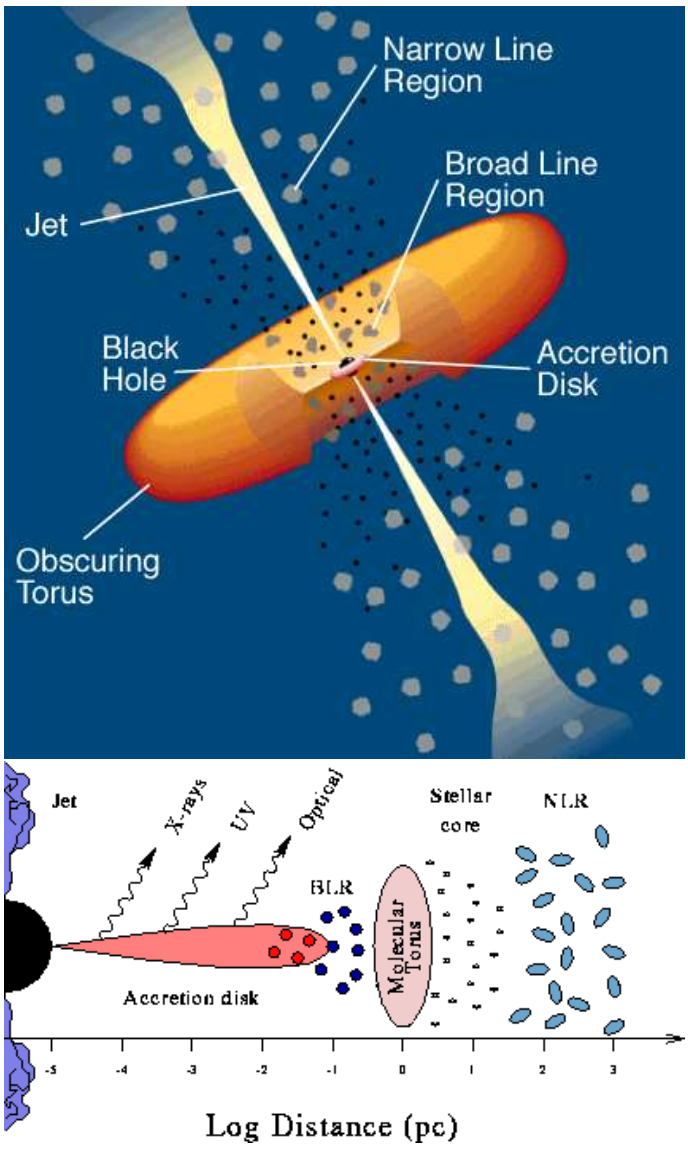

FIGURE 1.1: Up: Artistic representation of the Unified Model of AGN (credit: C.M. Urry and P. Padovani). Down: Skech of the componets of the Unified Model and its distance to the central SMBH (credit: K. Gebhardt webpage).

1. **Accretion disk:** The material falling into the SMBH forms a thin disk optically thick whose size is estimated to be of $\sim 10^{-2}$ pc. The disc emission is a multi-component black body of $T \sim 10^{5\pm1}$ K

2. **SMBH corona:** This is where the X-ray emission is originated and it is thought to be linked to the accretion disk forming a system. The hot plasma in the corona is hit by photons from the disk. A fraction of them, due to inverse Compton scattering, is reflected in the hard X-rays. This direct relation between the corona and the accretion disk is clear in the linear relation between the hard X-rays and the UV luminosity. Other photons are radiated back to the accretion disk. This contributes to maintain the accretion disk balanced and to form the corona-accretion disk system.

3. **Boad Line Region (BLR):** This region is formed by dust-free clouds of highly ionized gas. From the difference of line ratios from the core to the wings of the broad lines, it is indicated that this region is not a thin spherical shell (Crenshaw 1986). The material on the BLR is believed to form clouds orbiting at high velocities around the black hole. This clouds are thought to be at the far end of the accretion disk at a distance of 0.01-0.1 pc from the SMBH. The opening angle of this region is unknown to the date. This region explains the broad emission lines observed in the UV/optical spectrum with a large Doppler broadening of FWHM velocities of >1500 km/s. The emission of the disk ionizes this region producing the broad permitted lines in emission detected in the AGN spectrum. From line diagnostics, it is expected that its clouds are dense ($\sim 10^9$ cm^{-3}) and reaching temperatures of T$\sim$20000 K. For some objects there are detected other 'sub-regions' of the BLR, such as an intermediate line region (ILR) and a very broad line region (VBLR).

4. **Narrow Line Region (NLR):** The narrow lines observed in the UV/optical spectrum of AGN have FWHM velocities comparable to the host galaxy bulge stellar velocity. This lines are produced by the emission of gas clouds further away from the central engine ($\sim$100 pc), and hence, with lower ionization than in the BLR and not affected by variability. The lines produced in the NLR are forbidden and permitted lines that are excited by the accretion disk emission. From line diagnostics, it is expected that the clouds are less dense (10^3 cm^{-3}) and cooler (T$\sim$18000K) than the BLR. There is no transition region between the BLR and the NLR, they are completely separated regions in the AGN model.

5. **Torus:** Outside of the BLR, there is a dusty region with a toroidal geometry surrounding the black hole at a distance of $\sim$1 pc. This component is the key to explain the variations in the observed spectrum of the different AGN classes. Depending on the angle of view, covers the corona, accretion disk and BLR emission (in the case of a type-2 AGN), or gives a clear view of these central regions (type-1 AGN). More recent studies assume the dust to reside in clumps rather than being smoothly distributed. The nuclear emission is absorbed and scattered, and hence it heats the dust and re-emits it at NIR/FIR frequencies. This is not the only source of the emission at NIR/FIR, as dust also emits at these frequencies in the polar outflow of the AGN (Hönig *et al.* 2017).

6. **Radio Jet:** The jets are originated at the sub-parsec scales of the AGN and can often be traced up to distances of the order of kpc or Mpc. The radio emission is due to synchrotron emission of electrons ejected at relativistic energies in the polar direction. Large-scale jets are usually divided into FR I and FR II jets (Fanaroff and Riley 1974). FR I jets have low luminosity ($<10^{41}$ erg/s) that ends in radio lobes. FR II jets have a high luminosity ($>10^{41}$ erg/s) collimated jet that ends in hotspots.

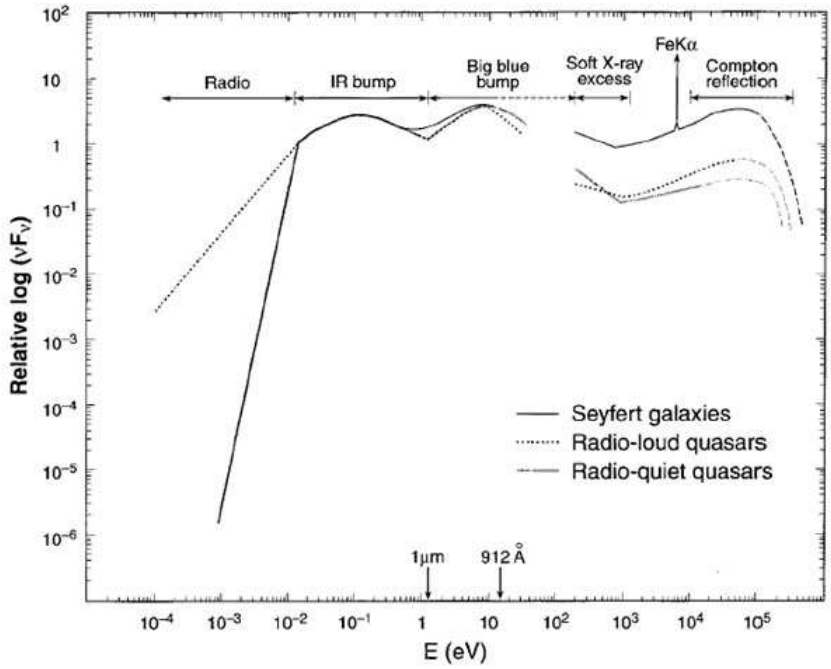

FIGURE 1.2: Typical SED of a few types of AGN from Beckmann and Shrader (2012).

The different regions in the Unified Model emmits at different wavelengths due to different emission mechanisms. In the following section we explain the different contributions to the spectral energy distribution (SED) with respect to this model.

1.2 Physical mechanisms of emission

We pointed out that AGN are detected in a wide range of energy ranges. In this section we list and explain the AGN emission in each of the available observational windows, and where are originated taking into account the Unified Model described in the previous section. In Fig. 1.2 we show the complete SED of a normal AGN.

1. **Radio emission:** The radio spectrum is well described with a power law, indicating a non-thermal origin (synchrotron emission, see Sec. 1.2.1.2). There are two subclasses of active galaxies, that are Radio Loud (RL) AGN and Radio Quiet (RQ) AGN, depending on the ratio of the optical emission and the radio emission (see Sec. 1.3).

2. **IR emission:** the IR component is generally attributed to thermal emission from dust at a wide range of temperatures (~ 50 -1000 K). This is called the IR bump. The inflection at the blue side of the Bump is produced at ~1 μm. This would correspond to the maximum temperature which dust could survive, that is around 1000-2000 K, depending on the composition of the dust grains. The IR bump peaks at 60 μm and falls dramatically in the submillimetre until the radio

continuum. The radio emission, with respecto to this IR emission, drops in flux about 5-6 orders of magnitude for RQ AGN, or roughly 2 orders for RL AGN

3. **UV/optical emission:** The shape of the UV/continuum emission can be modeled with a multi-component black body of T~$10^{5\pm1}$K. This is feature of the SED is called the Big Blue Bump (BBB), and usually is the peak of the AGN luminosity. The relative strengths of the IR and Big Blue bumps are generally comparable, but is not the same for all AGN. Superimposed to this featureless continuum there are permitted emission lines, with full width at half-maximum (FWHM) velocities of >1000 km/s from the Broad line region, and both permitted and forbidden and other emission lines with FWHM velocities comparable with the ones of the stellar at the bulge. In addition, there are blends that form pseudo continuum regions originated by two elements: one is the FeII pseudo continuum, with velocities comparable to the ones of the broad lines or slightly lower, and the continuum produced the by the high order Balmer lines. In particular there is a bump at the wavelength region of the MgII line called the Small Blue Bump, that is formed by a combination of those two blends.

4. **X-ray emission:** The emission in the X-rays is mainly a power law emission extending from 1keV to over 100 keV. In the energy space the flux can be modeled with a power law $F_E \sim E^{-\Gamma}$, being the photon index around $\Gamma \sim 1.9$. Below 2 keV, an emission excess is visible in the X-ray continuum (the 'soft excess') in 30% of AGN. The origin is not clear, but is sometimes associated to thermal emission linked to the accretion disk or collisionally-ionized diffuse gas. At energies harder than 10 keV, it is sometimes detected the presence of an exponential term that peaks around 80-300 keV and a bump that peaks at 30 keV (the 'Compton reflection hump'). This spectral feature is often explained as reflection of the direct X-ray continuum in the accretion disk or the molecular torus (Turner and Miller 2009). For some AGN it is visible a strong emission line at 6.4 keV, that is the fluorescent Fe Kα line.

5. **Gamma ray emission:** Blazars, a subclass of AGN, emits the majority of the bolometric luminosity above 100MeV. The spectrum of this sources is characterized by a non-thermal continuum, a flat radio spectrum and a featureless optical spectrum with strong variability and polarization.

The main ingredient for the conversion of the gravitational energy to emission is the accretion of material into the SMBH. Comparing the bolometric luminosity of the AGN with the maximum luminosity that the SMBH can irradiate (the Eddington luminosity, L_{Edd}), we can estimate the accretion of the AGN (the Eddington ratio, λ), assuming normally accretion efficiencies of about $\epsilon \sim 0.1$. In the literature we can find objects accreting at very low Eddington ratios (λ=10^{-2}-10^{-3}) to objects emitting at super-Eddington ratios (Raimundo and Fabian 2009).

This thesis focus more in the X-ray and UV/optical emission, so below we are explaining in a deeper way the emission mechanisms responsible of the emision at these energies. In Fig. 1.3 we are showing

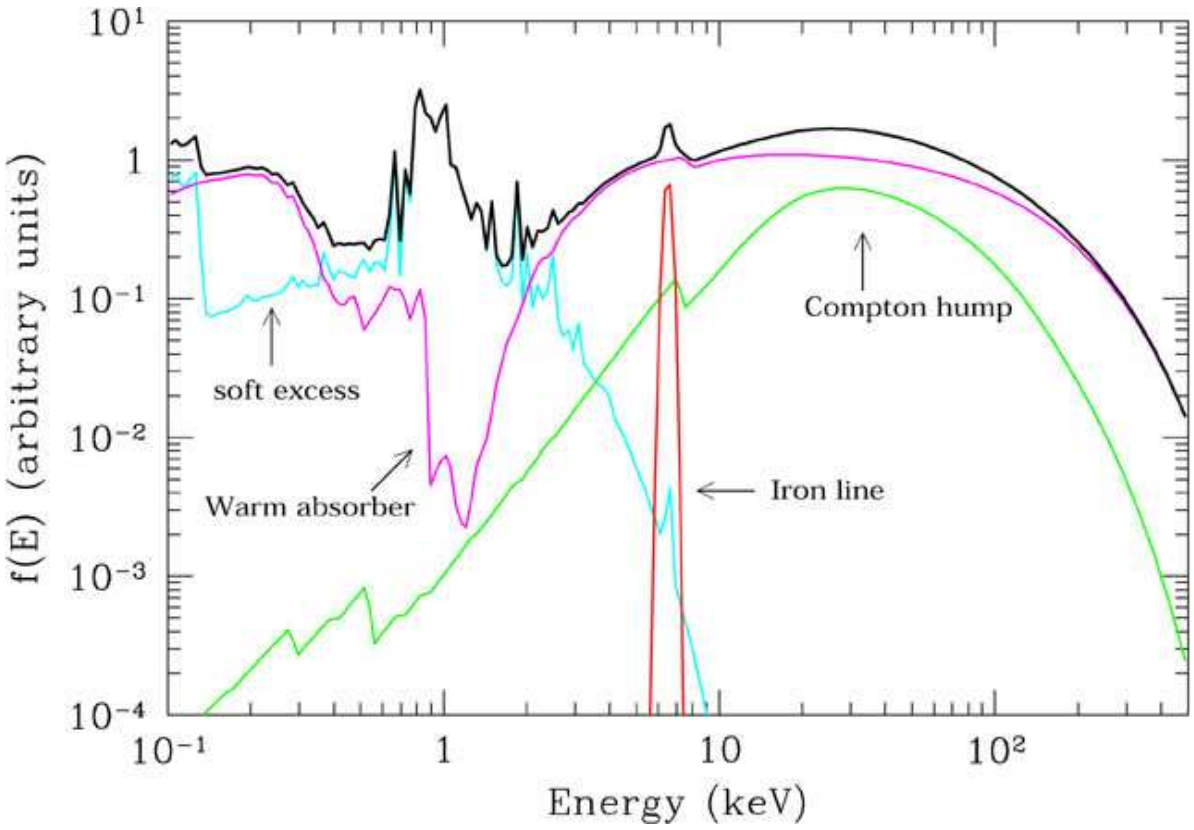

FIGURE 1.3: X-ray spectrum for a normal AGN, with the different components of the X-ray emission overplotted with different colors. Figure from Risaliti and Elvis (2004).

the components of the X-ray emission of an AGN. In Fig. 1.4 we are showing composite AGN spectra from Shen (2016) to help to understand the intrinsic UV/optical emission of an average AGN.

1.2.1 Primary X-ray emission

1.2.1.1 Free-free emission

Also called Bremsstrahlung emission, this is produced when free electrons are accelerated or decelerated in the Coulomb field of an atomic ionized nuclei and radiate energy. When a charged particle approaches to other one it will be deflected, and hence it will change the movement by accelerating or decelerating. This change of momentum of the two charges will provoke the emission of a photon whose amplitude is proportional to the charge of the two interacting particles in this process. In AGN this emission could be originated in a hot ionized gas near the SMBH. The medium of the BLR could be opaque to the free-free radiation meanwhile low density nebulae are optically thin to this radiation (Netzer 1990).

1.2.1.2 Sycrotron emission

This is the radiation produced when the charged particles are accelerating at relativistic velocities in a magnetic field. The particle changes direction due to the perpendicular force. The photon emitted is proportional to the energy of the electron, the magnetic field, and the angle between those two vectors.

1.2.1.3 Inverse Compton scattering

The inverse Compton scattering is the main contribution to the X-ray emission. This is produced by the interaction of low energy photons with high energy electrons, resulting in a gain of energy by the photons. The photons from the accretion disk that are emitted in the UV/optical energies interact with the electrons in the hot corona of the SMHB moving at relativistic energies. The emission of this phenomena is a power-law X-ray spectrum with a typical slope of Γ=1.9 (Caccianiga *et al.* 2004, Galbiati *et al.* 2005, Mateos *et al.* 2005b, Mateos *et al.* 2005a, Tozzi *et al.* 2006, Mateos *et al.* 2010, Corral *et al.* 2011).

1.2.2 X-ray reflection

X-ray photons at lower energies tends to be more absorbed than scattered, meanwhile photons at hard energies are more likely to be reflected. This provokes that the reflection spectrum of an AGN is a bump between 5-10 keV peaking at ~30 keV, that produces a flattening of the spectral slope at hard energies.

1.2.3 Fe emission line

There is often detected an emission line at 6.4 keV. This is the Fe-K line of the transition n=2-1 for ≤FeXVII. The presence of this line is thought to be provoked by fluorescence in the inner part of the accretion disk. The typical EW of the line is 100 - 200 eV. The line has an asymmetrical profile with a red wing, but generally the X-ray spectra quality is not enough to show it.

1.2.4 Emission in the UV/Optical range

1.2.4.1 UV/Optical continuum

When matter approaches to a massive object with a high angular momentum, it falls forming an accretion disk. The disk has annuli at many different temperatures so it is a sum of many blackbody spectra with a T_{eff} ~10^5 K, that peakes at the UV/optical. This is the origin of the featureless blue continuum

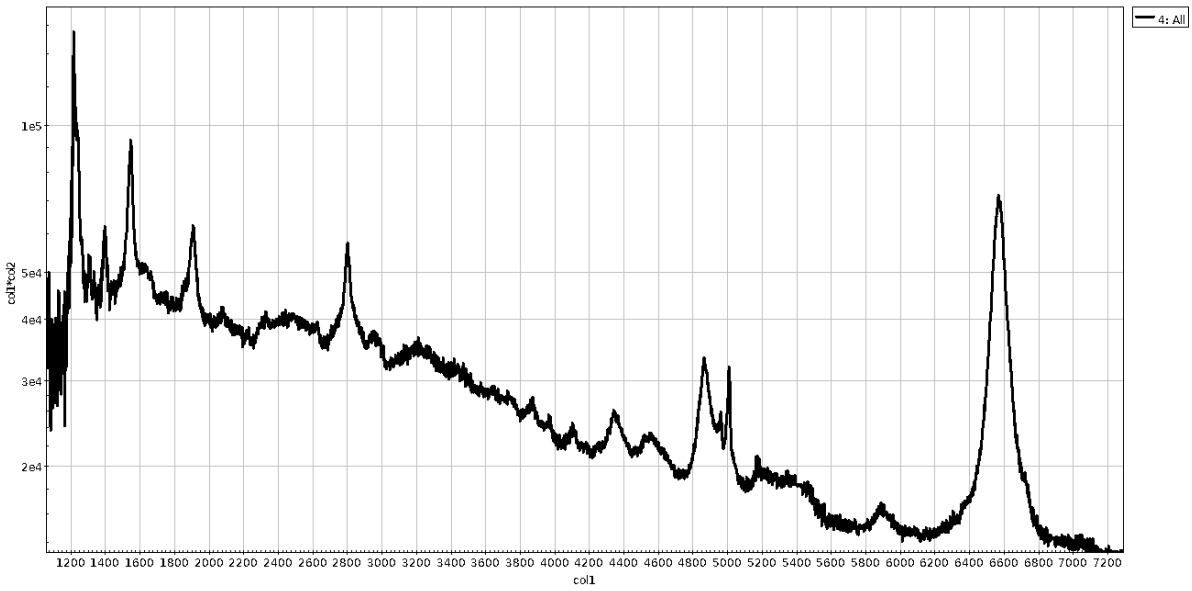

FIGURE 1.4: UV/optical QSO template from Shen (2016). TEMPORAL.

in the spectrum of an AGN. Redwards 10000 Å, the continuum slope changes due to the emission from the IR bump originated in the torus. The emission off AGN in the UV/optical range is compound by a sum of a featureless continuum from the accretion disk, and emission lines from the NLR and the BLR. The other continuum contributions are blends of emission lines (like FeII) and bound-free pseudocontinuum of the Balmer lines, that are explained in the following section.

1.2.4.2 Emission lines

The most likely source of power for the UV/optical AGN emission lines to be produced is the photoionization (Netzer 1990). The origin of the radiation that ionizes the material is the direct UV radiation of the disk. For the broad lines there are models that separates the region where the low ionization (Balmer lines, FeII, MgII) and high ionization (Ly$_\alpha$, CIV, CIII]) lines are emitted. The latter are likely emitted by a dilute outflowing medium, while the low ionization broad lines come mainly from material located at the outer regions of the accretion disk (Netzer 1990). The narrow line spectrum of type-1 and type-2 are very similar, but in some type-1 AGN there are much stronger highly ionized lines, that are emitted closer to the central engine (Ferguson, Korista, and Ferland 1997).

In this thesis we are focusing more in a wavelength range redwards ~2000 Å. In this region the most conspicuous broad emission lines are, from blue to red wavelength rest-frame core of the line, MgII, H$_\beta$ and H$_\alpha$. There are other broad emission lines, but they are less prominent, such as the ones from the Balmer series of the Hydrogen, and in the infrared, the ones from the Paschen series. The FeII emission comes from the outer parts of the BLR, as they are usually found to have FWHM velocities of 0.8-1.0 times the H$_\beta$ ones (Osterbrock 1991). They form a pseudo continuum, that is most prominent in the region of the MgII line (the Small Blue Bump, SBB), and two small regions bluewards and

redwards H_β. Nearly all broad line AGNs have optical FeII emission in their spectrum. The FeII strength is usually measured by the quantity R4570=FeII λ4570/H_β, being FeII λ4570 the flux of the FeII contribution measured between λ=4434-4684 Å and H_β the one of the total H_β contribution. As mentioned in Véron-Cetty and Véron (2000), this ratio is ~0.1-1 for the vast majority of objects. Only a 5% of AGN have R4570>1. Other pseudocontinuum from the BLR is the one formed by the stacking of the high order Balmer lines and bluewards 3646 Å the bound-free Balmer Continuum. This contribution appears in the SBB, along with part of the FeII emission. Normally. The forbidden narrow emission lines that are most prominent are the ones from the [OII] line, the [OIII] emission near H_β, the [OI] line, and the doublets near H_α from [NII] and [SII] elements. In addition, in the spectrum there are visible the narrow emission lines of the Hydrogen Balmer series.

The emission lines have the shape of a lorentzian profile. The velocity dispersion of the emitted material makes that the shape of the line is a gaussian profile due to Doppler broadening, as it is the dominant contribution to the width. For the broad emission lines, the centre of the line is displaced with respect to the rest-frame (Sulentic, Marziani, and Dultzin-Hacyan 2000, Steinhardt *et al.* 2012, Gaskell and Goosmann 2013). The narrow lines are not displaced but sometimes due to outflows it can be detected an extra blue component in addition to the rest frame narrow emission lines.

This are the general and most prominent characteristics of AGN emission. Nevertheless, active galaxies present a great variety of spectra. The presence or absence and the relative strength of some of the features shown in this section leads to different AGN classifications.

1.3 Classification of AGN

Given the Unified Model mentioned in Sec. 1.1 the observed spectra will depend on the orientation of the source with respect to the observer. The emision of AGN is detailed in Sec. 1.2, but some of the features may be obscured or not present in the spectrum. This leads to a vast variety of classes of AGN. In this section we will detail the different classifications in the AGN zoo putting them in context with the Unified Model and the radiation that is detected by the observer. To help the reader to understand the differences and the variety of AGN classes we include a scheme in Fig. 1.5.

In the literature it can be found a wide variety of AGN classes and subclasses. This vast variety can be explained by a variation on very small number of parameters, such as orientation (see Sec. 1.1), luminosity, variability, relative emission in some wavelengths windows, presence or absence of broad and narrow emission or absorption lines and host galaxy contribution. In Table 1.1 we show some of the classes seen in the literature.

As mentioned in Sec. 1.2, AGN are divided into Radio Loud (RL) and Radio Quiet (RQ) based on the relative strength of the radio emission. This is based on the relative radio emission based on the radio loudness parameter R. This is the ratio of the 5 GHz flux to the optical (B-band) emission. RL AGN

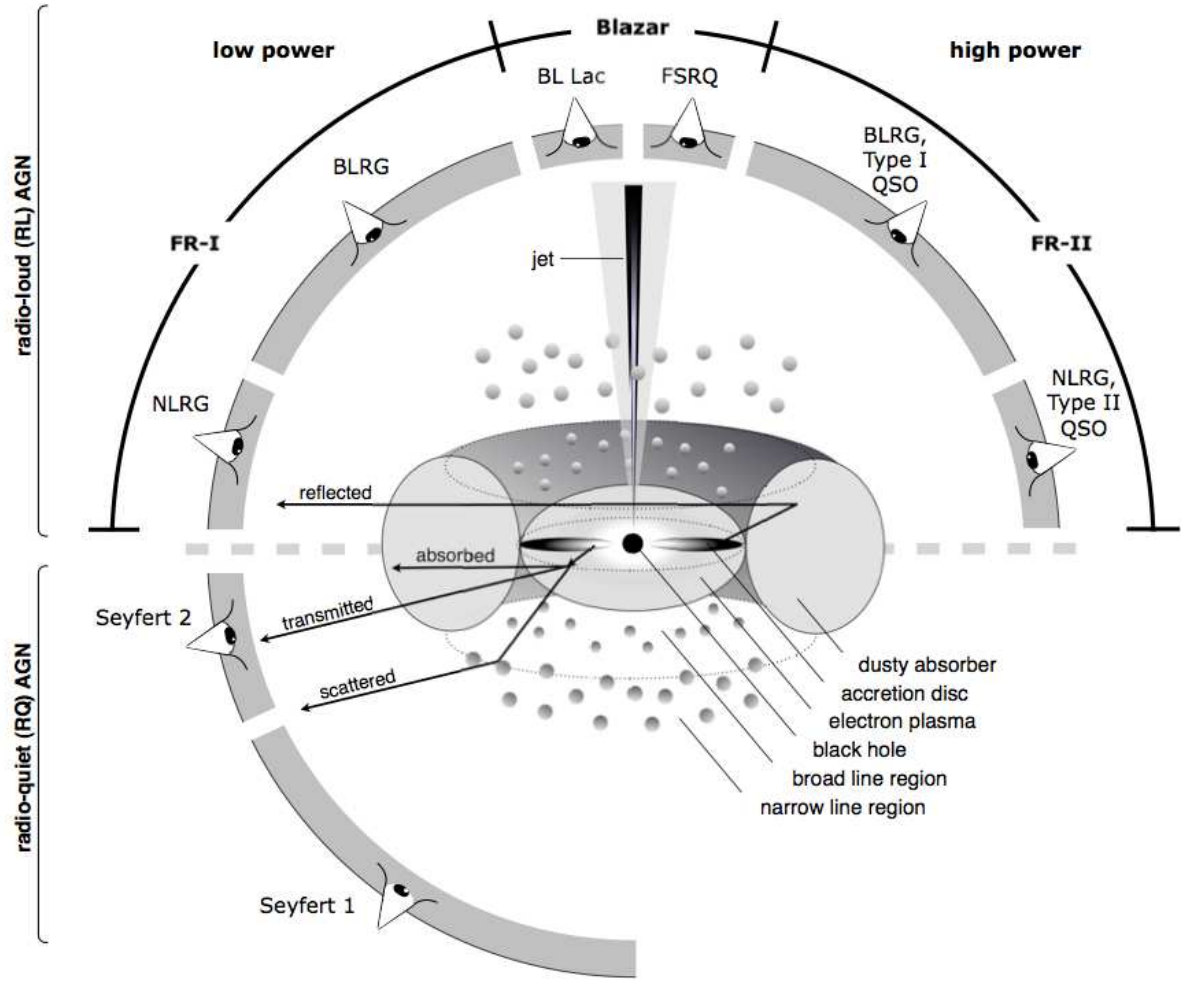

FIGURE 1.5: Schematic representation of the Unified model of AGN from Beckmann and Shrader (2012) and the different classification of the AGN incoming radiation depending on the viewing angle.

are the ones that the ratio R is larger than 10, and are approximately a 10 percent of the total AGN population. Radio emission for RL is between 2 and 4 orders of magnitude larger than the RQ AGN.

Other division is made in terms of the luminosity, that is the distinction between Seyfert galaxies and Quasar (QSO), to most luminous class of AGN. If the source have a magnitude in the B band higher than M_B <-21.5 mag, the AGN can be considered as a Quasar.

In this thesis we are focusing more in the classifications based on the X-ray and UV/optical wavelengths. The principal division at these energies is between type-1 and type-2 AGN. In the optical spectrum, a type-1 AGN is the one that shows broad emission lines with FWHM$\gtrsim$1000 km/s, edited in the BLR. Additionally, the optical spectrum presents narrow emission lines whose widths are comparable with the stellar velocity dispersion of the spheroidal component. The continuum from the accretion disk as it is low or not extinguished, is blue and frequently is more luminous than the host galaxy emission. Type-2 AGN show an optical spectrum that shows only narrow emission lines superimposed

Table 1.1: The AGN zoo: list of AGN classes.

Class/Acronym	Meaning	Main properties/reference
Quasar	Quasi-stellar radio source (originally)	Radio detection no longer required
Sey1	Seyfert 1	FWHM $\gtrsim 1000$ km s^{-1}
Sey2	Seyfert 2	FWHM $\lesssim 1000$ km s^{-1}
QSO	Quasi-stellar object	Quasar-like, non-radio source
QSO2	Quasi-stellar object 2	High power Sey2
RQ AGN	Radio-quiet AGN	see ref. 1
RL AGN	Radio-loud AGN	see ref. 1
Jetted AGN		with strong relativistic jets; see ref. 1
Non-jetted AGN		without strong relativistic jets; see ref. 1
Type 1		Sey1 and quasars
Type 2		Sey2 and QSO2
FR I	Fanaroff-Riley class I radio source	radio core-brightened (ref. 2)
FR II	Fanaroff-Riley class II radio source	radio edge-brightened (ref. 2)
BL Lac	BL Lacertae object	see ref. 3
Blazar	BL Lac and quasar	BL Lacs and FSRQs
BAL	Broad absorption line (quasar)	ref. 4
BLO	Broad-line object	FWHM $\gtrsim 1000$ km s^{-1}
BLAGN	Broad-line AGN	FWHM $\gtrsim 1000$ km s^{-1}
BLRG	Broad-line radio galaxy	RL Sey1
CDQ	Core-dominated quasar	RL AGN, $f_{\rm core} \geq f_{\rm ext}$ (same as FSRQ)
CSS	Compact steep spectrum radio source	core dominated, $\alpha_{\rm r} > 0.5$
CT	Compton-thick	$N_{\rm H} \geq 1.5 \times 10^{24}$ cm^{-2}
FR 0	Fanaroff-Riley class 0 radio source	ref. 5
FSRQ	Flat-spectrum radio quasar	RL AGN, $\alpha_{\rm r} \leq 0.5$
GPS	Gigahertz-peaked radio source	see ref. 6
HBL/HSP	High-energy cutoff BL Lac/blazar	$\nu_{\rm synch\ peak} \geq 10^{15}$ Hz (ref. 7)
HEG	High-excitation galaxy	ref. 8
HPQ	High polarization quasar	$P_{\rm opt} \geq 3\%$ (same as FSRQ)
Jet-mode		$L_{\rm kin} \gg L_{\rm rad}$ (same as LERG); see ref. 9
IBL/ISP	Intermediate-energy cutoff BL Lac/blazar	$10^{14} \leq \nu_{\rm synch\ peak} \leq 10^{15}$ Hz (ref. 7)
LINER	Low-ionization nuclear emission-line regions	see ref. 9
LLAGN	Low-luminosity AGN	see ref. 10
LBL/LSP	Low-energy cutoff BL Lac/blazar	$\nu_{\rm synch\ peak} < 10^{14}$ Hz (ref. 7)
LDQ	Lobe-dominated quasar	RL AGN, $f_{\rm core} < f_{\rm ext}$
LEG	Low-excitation galaxy	ref. 8
LPQ	Low polarization quasar	$P_{\rm opt} < 3\%$
NLAGN	Narrow-line AGN	FWHM $\lesssim 1000$ km s^{-1}
NLRG	Narrow-line radio galaxy	RL Sey2
NLS1	Narrow-line Seyfert 1	ref. 11
OVV	Optically violently variable (quasar)	(same as FSRQ)
Population A/B		ref. 12
Radiative-mode		Seyferts and quasars; see ref. 9
RBL	Radio-selected BL Lac	BL Lac selected in the radio band
Sey1.5/1.8/1.9	Seyfert 1.5, 1.8 or 1.9	ref. 13
SSRQ	Steep-spectrum radio quasar	RL AGN, $\alpha_{\rm r} > 0.5$
USS	Ultra-steep spectrum source	RL AGN, $\alpha_{\rm r} > 1.0$
XBL	X-ray-selected BL Lac	BL Lac selected in the X-ray band
XBONG	X-ray bright optically normal galaxy	AGN only in the X-ray band/weak lined AGN

Table extracted from Padovani *et al.* (2017). The top part of the table relates to major/classical classes. The last column describes themain properties. When these are too complex, it gives a reference to the first paper, which defined the relevant class or, when preceded by "see", a recent paper, which gives up-to-date details on it. Reference key: 1. Padovani (2016); 2. Fanaroff and Riley (1974); 3. Giommi *et al.* (2012); 4. Weymann, Carswell, and Smith (1981); 5. Ghisellini (2010); 6.O'Dea, Baum, and Stanghellini (1991); 7. Padovani and Giommi (1995); 8. Laing et al. (1994); 9. Heckman and Best (2014); 10. Ho (2008);11. Osterbrock and Pogge (1985); 12. Sulentic *et al.* (2002); 13. Osterbrock (1981).

to the host galaxy spectrum. The broad emission lines in this case are obscured and so not detected in the spectrum. The continuum from the accretion disk is reddened and its emission is obscured as well.

The type-1 Seyfert galaxies are also divided in terms of the FWHM of the H_β and FeII emission. When the FWHM of the broad H_β line is less than 2000 km/s, the H_β/[OIII]<3, and there is significant contribution of FeII. However, as discussed in Véron-Cetty and Véron (2000) and references therein, this division is rather arbitrary.

AGN emission features can be partially or totally outshined by stellar light from the galaxy (Severgnini *et al.* 2003, Georgantopoulos and Georgakakis 2005, Caccianiga *et al.* 2007, Caccianiga *et al.* 2008). Even that is normal that AGN contribution is the one that is more powerful in general, there are low luminosity AGN whose features are hard or impossible to measure. If these low luminosity sources have some level of extinction, its emission will be even harder to detect. This could make the source to be misclassified, or to be labeled as an XBONG.

In the X-rays, the Unified Model assumes that the differences between type-1 and type-2 results from the amount of absorbing gas in the line of sight. There is no consensus in the limit to divide between type-1 and type-2. From Caccianiga *et al.* (2008), it is used the limit $N_H > 4\times10^{21} cm^{-2}$ cm^{-2}, that comes from the limit A_V =2 mag, that normally obscures the broad lines in the spectrum. Other studies find the limit in $N_H > 10^{22} cm^{-2}$ (Ueda *et al.* 2003), and use this more conservative limit to ensure that this extinction is intrinsic from the AGN and does not come from Galactic gas .

There is as well subdivisions in the type-1/type-2 classifications, due to the fact that there are intermediate types with detectable but weak broad emission lines. The relative strength of the broad lines with respect to the narrow lines that can not be explained simply by type-1 or type-2 provoked the need to add a subclassification. In this thesis we subclasiffy the AGN into type-1.0/1.2/1.5/1.8/1.9 following the scheme from Whittle (1992):

- **Seyfert 1**: Objects showing broad H_β emission line and with [O III]/H_β < 0.3
- **Seyfert 1.2:** Objects showing broad H_β and with 0.3 < [O III]/H_β < 1
- **Seyfert 1.5:** Objects showing broad H_β and with 1 < [O III]/H_β < 4
- **Seyfert 1.8:** Objects showing broad H_β and with 4 < [O III]/H_β
- **Seyfert 1.9:** Objects not showing broad H_β, but having broad H_α
- **Seyfert 2:** Objects without H_α nor H_β broad-line emission

This subclassification due to the relative strength of the broad lines with respect to the narrow line emission has a direct relation with the partial obscuration of the central parts of an AGN. The strength

of the broad emission, emitted in regions close to the SMBH, is partially extinged from the torus. Meanwhile, narrow emission is emitted farer away from the SMBH, less affected by obscuration.

Additionally, as mentioned in Véron-Cetty and Véron (2006), in the literature are examples of objects without UV/optical broad emission lines detected, but that they show Paschen broad emission lines in the infrared (Goodrich, Veilleux, and Hill 1994). This sources are classified as S1i, and this is explained because in this sources the high dust extinction make the UV/optical lines undetectable, but in the infrared, less affected by dust extinction, they can be detected. There are as well the S1p class, that do not show broad emission lines, but they are detected in the polarized spectrum (Antonucci and Miller 1985, Miller and Goodrich 1990, Tran, Miller, and Kay 1992).

The observed radiation of an AGN is heavily affected by the obscuration of the material in the line of sight, so a good understanding on the extinction mechanisms is hence needed in order to explain the differences in the observed spectrum (ie. in classification) of active galaxies.

1.4 Absorption and obscuration

Once established the unified model of AGN, it is clear that the obscuration plays a main role in understanding the observed properties of AGN. The amount of obscuration in the line of sight will determine the classification in terms of type-1 or type-2. Understanding the absorption mechanisms in each band will help us to test the unified schemes and to recover the intrinsic properties of the active galaxies. To do so, in this section we explain the extinction models in the optical range and in the X-rays.

The radiation emitted has to go through various materials until it reaches us. First it must cross the surrounding material of the AGN. Depending on the orientation, it will pass different quantity and density of dust and gas. As it was explained in the previous section, the emission that propagates in the radial direction of the disk, will be absorbed by the BLR and the torus and will be completely blocked. Meanwhile, the radiation that propagates outside of the torus covering angles will escape through the AGN practically unaffected. Outside of the nuclei, it will be affected by material in the interstellar medium of the host galaxy, such as dust lanes or gas clouds. Finally, it will be absorbed by the Galactic extinction. This last contribution to the incoming extinction is know and can be corrected in X-rays using the NHI Galactic maps (Dickey and Lockman 1990) and in the UV/optical assuming a measured dust-to-gas relation of the Milky Way, and thus converting N_H to A_V.

Dust grains are the main ingredient responsible of UV/optical extinction via scattering and absorption of the emitted photons. As the effect of the scattering and absorption is more effective at wavelengths comparable to dust grains size (λ=2×π×a, being a the size of the dust grain), its effect is higher at lower wavelengths. Depending on the dust grains, the extinction can differ. In Fig. 1.6 we show different extinction models and the effect with the wavelength. There is as well a feature around 2175 Å that is the Carbon dip, that is explained by PAHs and graphite (Weingartner and Draine 2001). This

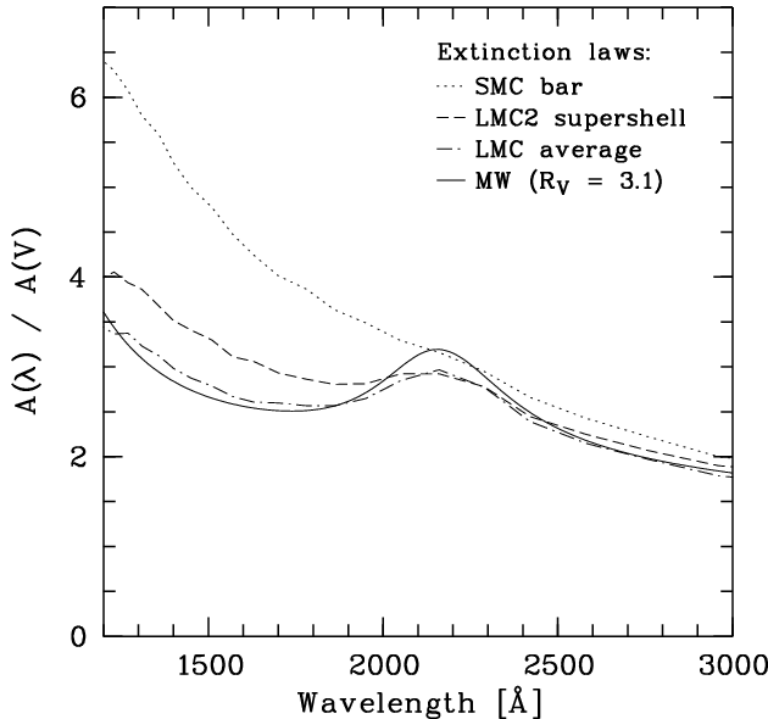

FIGURE 1.6: Different models of the ratios of dust extinction with respect to wavelength. Figure from Noll and Pierini (2005).

is detected in various models and absent in others. The dust. For QSO, the extinction model that best explain the reddening curve is the one from the Small Magellanic Cloud (Hopkins *et al.* 2004), being one of the most used the one from Gordon *et al.* (2003). The absence of the Carbon dip favours an scenario where the small grains coagulates forming bigger grains (Maiolino *et al.* 2001).

One of the methods used to measure the amount of optical reddening in the source is by computing the Balmer Decrements. This consists in compare the relative strengths of emission lines, mainly H_α and H_β, but other times it is used H_ϵ or even Paschen lines, and compare with the intrinsic relative strengths. For the most used case, that is H_α/H_β, we assume a case B recombination and optically thin photoionized plasma (Osterbrock 1989). The intrinsic value is normally assumed to be around 3.1 for the NLR and 3.4 for the BLR, without a clear and universally accepted value. Recent studies are finding that this value have a considerable spread (Jin, Ward, and Done 2012, Schnorr-Müller *et al.* 2016), as it depends on the conditions of the emitting region (Netzer 2013). Other method to estimate the extinction is fit the AGN continuum using an extinction model and an AGN template. This approach is no extent of inconvenients, as there are sources with a continuum intrinsically different than the average. There are a population of AGN whose continuum is redder than the average, and so the method can confuse intrinsically red object with a small amount of reddening in the source.

In a first order, the principal component that absorbs the X-ray photons is the gas in the line of sight, and within the gas, the hydrogen is the predominant element that contributes to obscure the X-ray

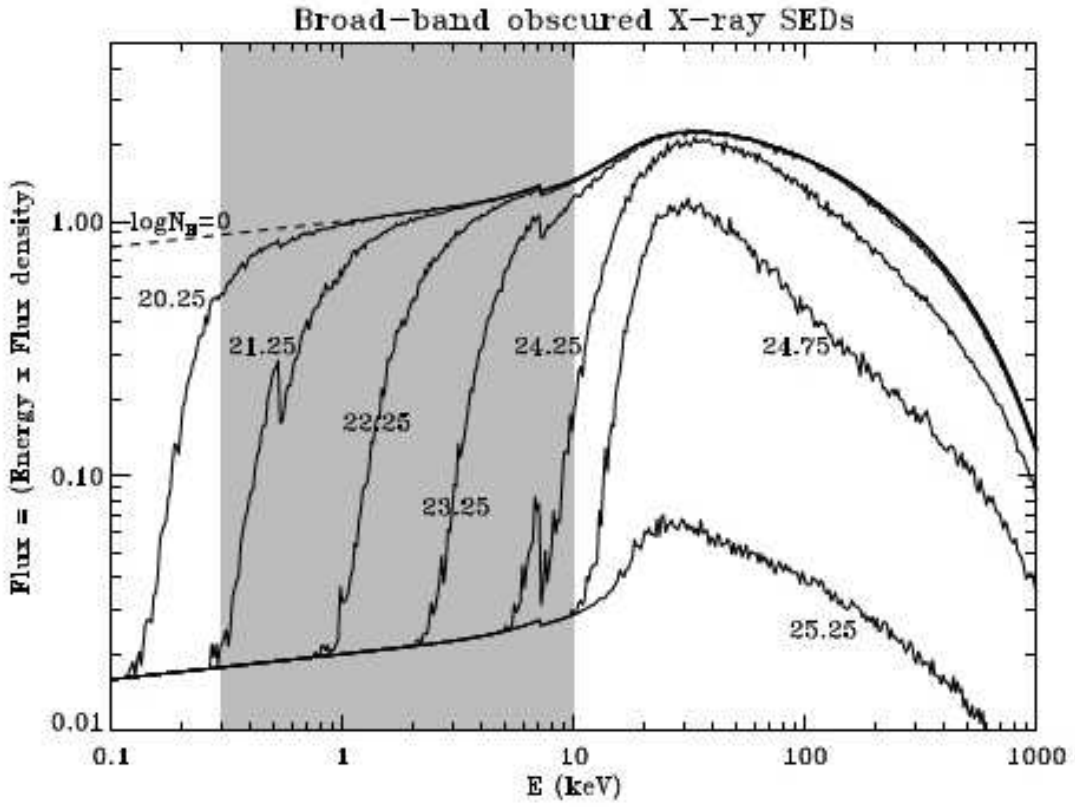

FIGURE 1.7: The effect of gas absoption in the X-ray emission. Figure from the adaptation of Wilman and Fabian (1999) shown in Singh (2013).

emission. This is why the X-ray absorption is quantified in terms of the N_H column density. The probability for an X-ray photon to be absorbed follows Eq.1.1:

$$P(E) = 1 - e^{(-\sigma(E)\times N_{\rm H})} \tag{1.1}$$

Where σ(E) is a the cross section of the photoelectric absorption. The effect of the gas to the X-ray photons is higher at soft energies. In Fig. 1.7 we show the effects on a simple power law with different levels of gas in the line of sight.

According to the Unified Model, one source with significant extinction in the optical range should appear as absorbed in the X-rays and vice versa, but this is not happening for 10-20% of the sources. This fraction of discordant AGN appears indepently of the selection method (eg. Panessa and Bassani 2002, Caccianiga *et al.* 2004, Mateos *et al.* 2005b, 2005a, Mainieri *et al.* 2005, Caccianiga *et al.* 2008, Mateos *et al.* 2010, Corral *et al.* 2011, Scott, Stewart, and Mateos 2012, Page *et al.* 2011, Merloni *et al.* 2014). The mismatch between optical extinction and X-ray absorption described above is observed in both optical/infrared and X-ray selected samples at all redshifts. The origin of such apparent discrepancies remain unclear, and hence so it is the validity of the unified model for such AGN.

There has been many attempts to explain the origin of the discrepancies for X-ray unabsorbed and optically type-2 AGN. For some AGN it is found that there is more dust in relation with the gas, although such cases are very rare (Caccianiga *et al.* 2004, Trippe *et al.* 2010, Huang *et al.* 2011, Malizia *et al.* 2012, Masetti *et al.* 2012, Mehdipour, Branduardi-Raymont, and Page 2012), so in this cases, the emission from the X-rays would arrive to us practically unaffected by the material in the line of sight, and the optical emission will be obscured. Other possibility is that the broad UV/optical lines are diluted by the host galaxy starlight, so in this case the source is classified as a type-2 AGN as there is not enough signal-to-noise to distinguish AGN features from the stellar emission. This is the case of XBONGS. In other objects, optical observations show an intrinsically high Balmer decrement for the Hydrogen broad emission lines, while the X-ray spectra show low absorption (Barcons, Carrera, and Ceballos 2003). A dusty-ionized absorber can produce more relative absorption in the X-rays than in the optical emission (Della Ceca *et al.* 2001).

Compton-thick AGN can be misclassified as an unabsorbed type-2 AGN, since the direct X-ray emission below 10 keV is completely absorbed and we would only detect scattered nuclear radiation (Braito *et al.* 2003, Akylas and Georgantopoulos 2009, Braito *et al.* 2011, Malizia *et al.* 2012), which might be mistaken by direct emission. This emission is about 1-3% of the total X-ray emission (Gilli, Salvati, and Hasinger 2001, Comastri 2004, Georgantopoulos *et al.* 2011a), therefore comparing it to the luminosity at other energies (eg. the [OIII] line) can unveil if the source is a compton thick or not. Scattered nuclear radiation would have a lower power law index as well. The EW of the Fe line at 6.4 keV would be high as well due to the relative difference between the strength of the line and the scattered nuclear radiation.

High gas-to-dust ratios could be a possible answer to high absorbed AGN in the X-rays but showing low or not extinction at UV/optical energies . The gas-to-dust ratios can increase due to dust sublimation close to the central X-ray source (Granato, Danese, and Franceschini 1997). Other explanation is that dust grains are biased to be bigger in the environment of AGN, more specifically small grains of dust coagulates forming larger grains (Maiolino *et al.* 2001), an explanation more plausible than the destruction of small grains in favour of larger grains, especially given that the PAHs from the Carbon dip at 2175 Å is not normally present in AGNs (Hopkins *et al.* 2004). Eclipsing material coming from the dust-free BLR can as well act as an additional absorption of the X-ray photons leaving UV/optical photons less affected. As the angle of aperture of the BLR is not known, nor if is similar in all AGNs, this could be a valid scenario to explain this sources.

An independent explanation without having to invoke to non standard physics or obscuring material is that there is variability in the sources. If the optical and X-ray data has been taken at different dates, we can not discard that the discrepancies are originated by eclipses of gas and/or dusty clouds in the line of sight. The clumpy structure model of the BLR and the torus would be compatible with this explanation. In fact, there are reports in the literature of changing look sources (LaMassa *et al.* 2015, Miniutti *et al.* 2014). Even considering variability with simultaneous optical and X-ray observations,

there are sources whose classification in these energies are discordant (Corral *et al.* 2005, Bianchi *et al.* 2008, 2012).

1.5 Aims of this thesis

Describe the aims of the papers in this thesis.

Summarizing, along this work we will tackle the following issues:

1. One
2. Two
3. Three

Chapter 2

Instrumentation

In Chap. 2 it was explained with detail the emission of AGN and its classification, derived from a great variety of spectral energy distributions. This fact makes the selection of an unbiased, uniform and complete sample of AGN an extremely difficult task. In order to perform a proper selection of active galaxies it is needed to understand the limits of each wavelength range.

AGN were in first place detected at radio frequencies being called them Quasi Stellar Radio sources (and after, Quasars or QSO), but only a small fraction of objects emits strongly in the radio band. In the optical band it is where the maximum of emission of the AGN is, optical surveys provide large samples of AGN, but the selection techniques dramatically misses reddened objects and even host galaxy dominated ones. Infrared selection techniques are the most efficient ones to detect sources that are highly obscured and missed in the rest of the spectral bands, but this works for high luminosity sources, as it is needed to distinguish between the host IR emission and the contribution from the dust heated from the AGN.

In this thesis we use an X-ray selection based on the 2-10 keV energies. This band is sensible to X-ray absorption up to the Compton Thick limit ($N_H \sim 10^{24}$ cm^{-2}). This AGN are found in the X-rays surveys identifying the counterparts in the optical for the X-ray sources, by cross-correlation of catalogs or by dedicated observations of the sources.

The selection used in this thesis is from the wide-angle (44.43 sq. degree) Bright Ultra-hard XMM-Newton Survey (Mateos *et al.* 2012). This is a flux limited ($f_{4.5-10\,\mathrm{keV}} \geq 6{\times}10^{-14}$ erg s^{-1} cm^{-2}) hard X-ray selected (4.5-10 keV) sample using the XMM-Newton observatory. The BUXS survey and the sample used are described in detail in Chap. 3.

This chapter will explain the instrumentation used to detect the active galaxies in the X-rays using XMM-Newton in Sec. 2.1 and in the optical in Sec. 2.2, and more precisely using long-slit spectra form dedicated observations (Sec. 2.2.1) and fiber spectra from public surveys (Sec. 2.2.2).

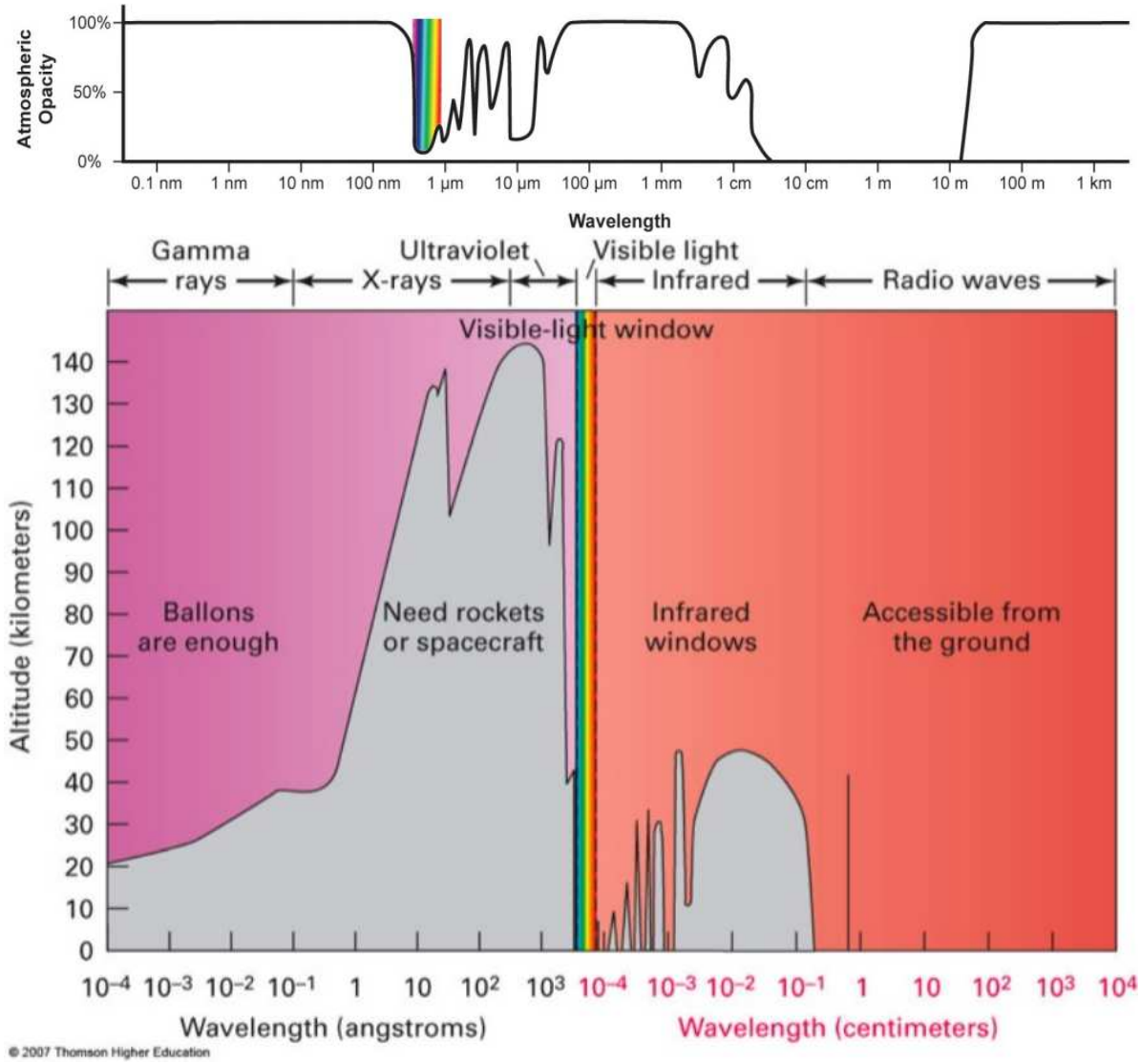

FIGURE 2.1: Top: Opacity of the atmosphere in terms of the observed wavelength (credit: NASA). Bottom: Altitude in kilometers in order to observe each wavelength range (credit: Thomson Higher Education 2007).

2.1 X-ray observations

The atmosphere of the Earth is completely opaque to photons of certain energy as seen in Fig. 2.1. For some of the wavelength bands, the detectors must be at a certain altitude in order to detect its radiation. Optical emission can be detected from instruments located at the ground, as well fro some infrared energy windows. But in order to collect data from X-ray emission it is needed to place detectors in rockets or space observatories.

In this thesis the X-ray data that is used comes from the X-ray Multi-Mirror satellite XMM-Newton. This is one of the four 'Cornerstone' missions defined in the Horizon 2000 Programme of the European Space Agency (ESA).

2.1.1 XMM-Newton

The spacecraft XMM-Newton was launched by an Ariane 504 from Kourou, French Guiana on 10 December 1999. The satellite is orbiting in a elliptical orbit around the Earth, with an inclination of 40^o, being the apogee at a distance between 99000 and 115000 km and the perigee between 6000 and 22000 km of altitude. The spacecraft takes 48 hours to complete an orbit.

The observatory XMM-Newton carries three scientific instruments, that are the European Photon Imaging Camera (EPIC; Turner *et al.* 2001, Strüder *et al.* 2001, see Sec. 2.1.1.1) the Reflection Grating Spectrometer (RGS; den Herder *et al.* 2001, see Sec. 2.1.1.2) and the Optical Monitor telescope (OM; Mason *et al.* 2001, see Sec. 2.1.1.3) that allows simultaneous optical and X-ray observations. In Fig. 2.2 it is shown a sketch of the XMM-Newton spacecraft.

The three X-rays telescopes are build with 58 Wolter I grazing-incidence mirrors, being the largest mirrors of 70 cm of diameter. They are nested in coaxial and cofocal configuration with a grazing angle of 30'. The focal length of these telescopes is 7.5 m. This configuration allows that the instruments can achieve a an effective area of $\sim$ 1500 cm^2 over a wide energy range (0.1-15 keV), in particular at energies close to the rest frame Fe Kα line.

2.1.1.1 European Photon Imaging Camera (EPIC)

The European Photon Imaging Camera (EPIC) are Charge-Coupled Device cameras (CCD) that can register extremely weak X-ray radiation and can detect flux variation in the range of microseconds. these advanced Charge-Coupled Device cameras (CCD) are capable of detecting rapid variations in intensity in the range of ~0.001 seconds.

They are located at the prime focus of each of the three telescopes. The EPIC camera have the following detectors, two Metal Oxide Semi-conductor (EPIC-MOS; Turner *et al.* 2001) and one EPIC-pn (Strüder *et al.* 2001). In front of the detector, it is located a filter wheel.

- The EPIC-MOS consists on two sets of CCDs sensible in the 0.1-15 keV energy range, with a moderate spectral energy resolution of E/ΔE=20-50. Each EPIC-MOS camera consist on a mosaic of 7 CCDs where each CCD is 600 $\times$ 600 pixels. Every single CCD have a size of 10.9' $\times$ 10.9', so the total Field of View of the MOS camera is 33' $\times$ 33'.
- There is only one unit of the EPIC-pn camera. This one is a mosaic of 12 CCDs (64 X 200 pixels each), with a FOV of 12.6' $\times$ 4.4' each one, to obtain a total FOV of 27.5' $\times$ 27.5'. As the EPIC-MOS cameras, this unit is sensible to the energy range of 0.1-15 keV with the same spectral resolution of E/ΔE=20-50.

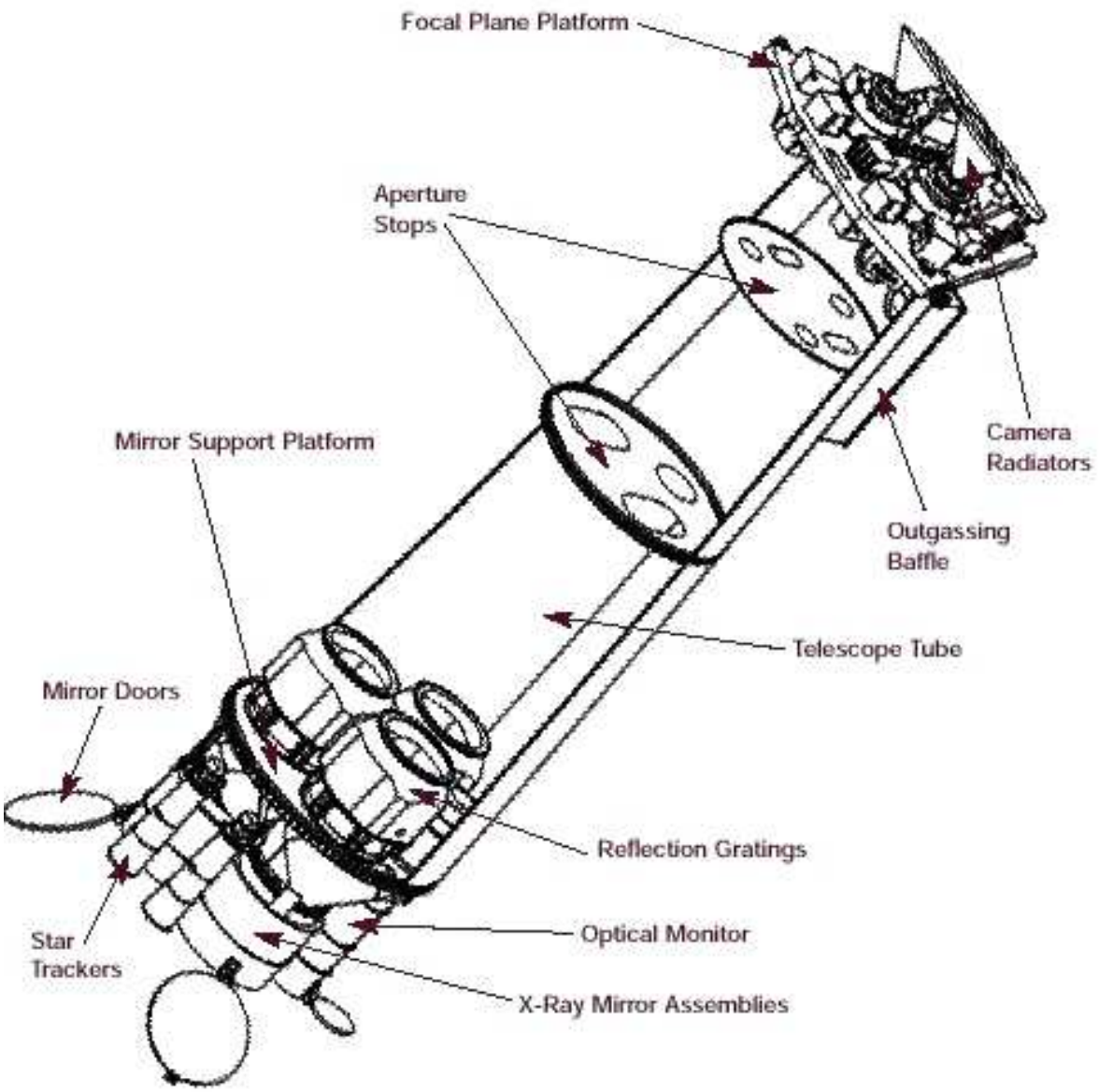

FIGURE 2.2: Diagram of the XMM-Newton spacecraft (credit: ESA).

2.1.1.2 Reflection Grating Spectrometer (RGS)

In two of the telescopes, roughly a 40 per cent of the incoming radiation is reflected to a secondary focus, where the Reflection Grating Spectrometers (RGS) are located. Those two RGS allows high resolution ($E/\Delta E$=100-500) for the soft X-ray energy range of 0.3 to 2.1 keV. The objective is to detect K-shell transitions of elements such as carbon, nitrogen, oxygen, neon, magnesium, and silicon and the L-shell transitions of iron.

TABLE 2.1: Filters available for the Optical Monitor.

Name	$\lambda_{eff}^{(a)}$ (Å)	$\lambda_{max}^{(b)}$ (Å)	FWHM (Å)	PSF_{FWHM} ('')	Peak mag (mag)
V	5407	5230	684	1.35	19.0
B	4334	3980	976	1.39	19.7
U	3472	3270	810	1.55	19.5
UVW1	2905	2680	620	2.0	19.3
UVM2	2298	2210	439	1.8	18.3
UVW2	2070	2000	500	1.98	17.6
WHITE$^{(c)}$					22.2

(a): Effective wavelength; (b): Wavelength of maximum transmission; (c): An ''open" filter.

2.1.1.3 Optical Monitor

The last instrument onboard is the Optical Monitor (OM), that is a 30 cm Ritchey-Chretien telescope that works on the wavelength range of 1800-6500 Å. It can collect images of the same regions as the X-ray telescope simultaneously with a FOV of ~ 17' and ~ 1" of spatial resolution. The filters available are listed in Table 2.1.

2.2 Ground based telescopes

In order to classify and identify all the X-ray sources, optical observations are made. Some of the optical counterparts comes from the SDSS public archive. Others are made using follow up observations of the X-ray sources by submitting a proposal to optical telescopes.

In Sec. 2.2.1 it is shown in detail the optical telescopes used to acquire the optical spectra for the X-ray sources.

2.2.1 Long Slit spectra from optical telescopes

2.2.1.1 VLT/X-Shooter

The Very Large Telescope (VLT) is operated by the European Southern Observatory (ESO) at Paranal Observatory in the Atacama Desert of Chile at 2635 m above sea level. It consists of four individual telescopes (UT1:Antu, UT2:Kueyen, UT3:Melipal, UT4:Yepun), each one with a diameter of the primary mirror of 8.2 m. The instrument X-Shooter, whose detailed description can be found in Vernet *et al.* (2011), is placed on the Cassegrain focus of the second telescope, UT2:Kueyen. In Fig. 2.3 we show an sketch of X-Shooter. This instrument consist in a combination of 3 echelle spectrographs that provides simultaneous UV-to-NIR spectroscopy (3000-25000 Å) with intermediate spectral resolution

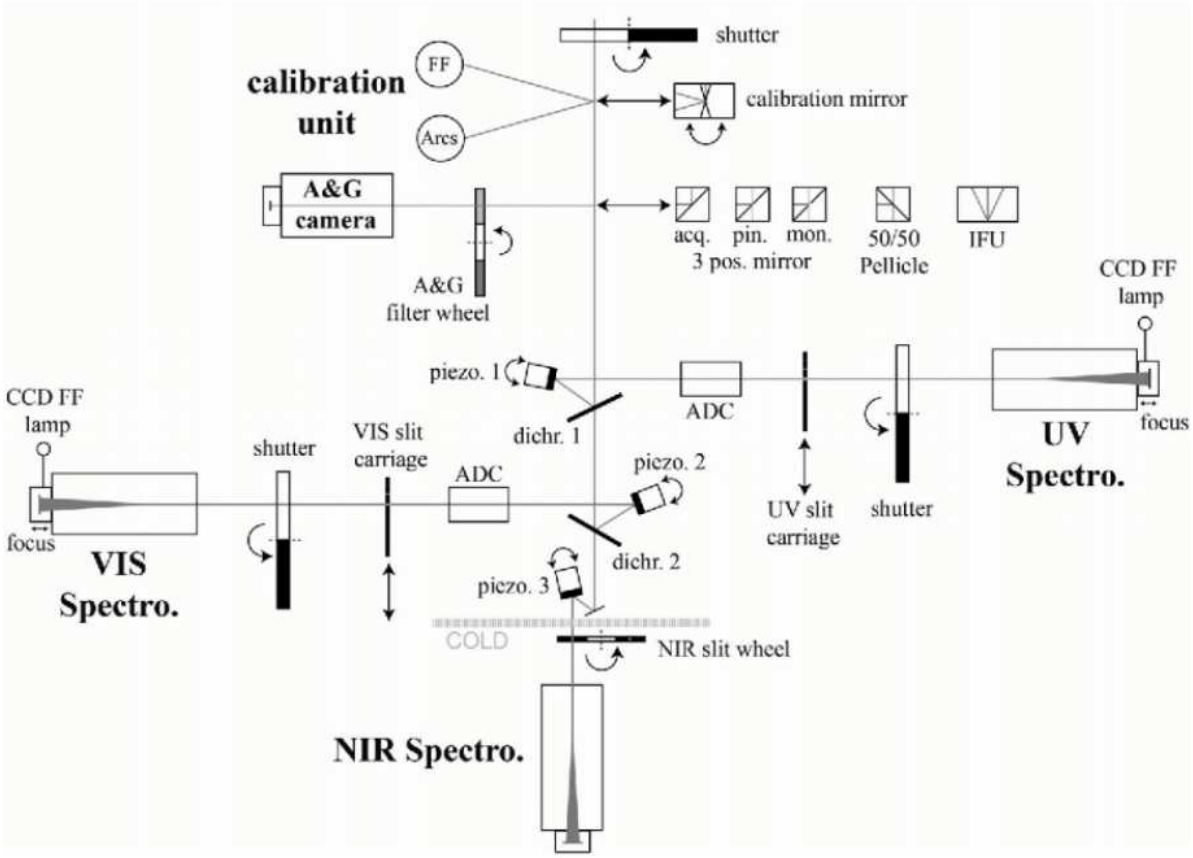

FIGURE 2.3: Schematic overview of VLT/X-Shooter (credit: ESO).

(R~4000-17000, depending on wavelength and slit width). The incident light is divided in three different paths through two dichorics, each one reaching a different echelle spectrograph. This is conducted using two dichorics, the first with a cut off od 5595 Å and the second for 10240 Å. One arm is for the UV light (UVB:3000-5595 Å), other for the optical (VIS:5595-10240 Å), and the last one for the near infrared (NIR:10240-24800 Å). Additionally UVB and and VIS optical paths incorporate an Atmospheric Dispersion Corrector (ADC) that allows to compensate the effects of differential atmospheric refraction. This allows to not to be restricted to orient the slit to the parallactic angle, as it will correct the refraction wavelength dependent slit losses independently from the airmass and the orientation of the slit. The effect on the infrared is low, so no NIR ADC is used in X-Shooter.

In this thesis we use VTL/X-Shooter for a detailed study of two AGN (See Chap. 4). The information setup about the used slit is shown in Table 2.2. All the slits have a fixed length of 11".

2.2.1.2 VLT/FORS2

The instrument FOcal Reducer/low dispersion Spectrograph 2 (FORS2) an instrument installed at the VLT telescope Antu (UT1), in the cassegrain focus. It can be used with multiple modes such as

TABLE 2.2: Used X-Shooter setup for the objects in this thesis.

Arm	Slit Width (‘’)	R ($\lambda/\Delta\lambda$)	Sampling (pix/FWHM)
UVB	1.0	5100	6.3
VIS	0.9	8800	6.0
NIR	0.9	5100	6.3

TABLE 2.3: VLT/FORS2 setup for long slit spectroscopy.

Grism name + ESO number	λ_c (Å)	Wavelength range (Å)	Dispersion (Å/mm)	R (foe 1” slit)
GRIS 600B+22	4650	3300-6210	50	780
GRIS 300V+10 (1)	5900	3300-(6600)	112	440
GRIS 300V+10	5900	4450-8650	12	440
GRIS 300I+11	8600	6000-11000	108	660
GRIS 150I+27 (1)	7200	3300-(6500)	225	260
GRIS 150I+27 (1)	7200	4450-(8800)	230	260
GRIS 150I+27	7200	6000-11000	230	260
GRIS 1400V+18	5200	4560-5860	20.8	2100
GRIS 1200B+97	4350	3660-5110	24.0	1420
GRIS 1200R+93	6500	5750-7310	25.0	2140
GRIS 1028z+29	8600	7730-9480	28.3	2560
GRIS 600RI+19	6780	5120-8450	55	1000
GRIS 600z+23	9010	7370-10700	54	1260

(1) If used without or with the listed order separation filter, the orders will overlap above the given wavelength.

imaging, polarimetry, and spectroscopy. In this last one, there are available various spectroscopic modes, that are a long slit spectroscopy, moveable slitlets, and an spectroscopic mask mode. In this thesis we only use the long slit spectroscopy mode (LSS).

The nine slits available in LSS mode have widths between 0.3” and 2.5”. The slit width is not variable. The wavelength range in FORS2 is between 3300 and 11000 Å, with an spectral reslution of R=260-2600 depending on the grism (see Table 2.3).

2.2.1.3 GTC/OSIRIS

The Gran Telescopio CANARIAS (GTC) is the largest optical telescope to date. The primary mirror of the GTC is formed by a set of 36 hexagonal mirrors that forms a mosaic of a mirror of 10.4 m of diameter. This telescope is placed at the Roque de los Muchachos Observatory on the island of La Palma, Spain, at 2396 m above sea level. The GTC was built by the public company GRANTECAN S.A., that also operates it.

TABLE 2.4: GTC/OSIRIS setup for long slit spectroscopy.

ID	λ_c (Å)	λ_{range} (Å)	D (Å/pix)	R	Peak Efficiency	Type
R300B	4405	3600 -7200	4.96	360	70%	Grism
R300R	6635	4800 - 10000	7.74	348	70%	Grism
R500B	4745	3600 - 7200	3.54	537	68%	Grism
R500R	7165	4800 - 10000	4.88	587	67%	Grism
R1000B	5455	3630 - 7500	2.12	1018	65%	Grism
R1000R	7430	5100 - 10000	2.62	1122	65%	Grism
R2000B	4755	3950 - 5700	0.86	2165	87%	VPH
R2500U	3975	3440 - 4610	0.62	2555	70%	VPH
R2500V	5185	4500 - 6000	0.80	2515	80%	VPH
R2500R	6560	5575 - 7685	1.04	2475	80%	VPH
R2500I	8650	7330 - 10000	1.36	2503	80%	VPH

The instrument that is used in this thesis for long slit spectroscopy is OSIRIS (Optical System for Imaging and low-Intermediate-Resolution Integrated Spectroscopy), located in the Nasmyth-B focus. This instrument uses slits with widths ranging from 0.4" to 10", and with a length of 7.4' for all of them. Ositis is composed by two CCDs. The objects that are being observed are centered in the coordinate X=200 of the CCD2 in order to minimize the cosmetic effects that could affect the spectrum, as CCD1 have more artifacts than CCD2. Osiris can operate with resolutions between R=300 to R=2500, covering wavelength ranges between 3650 and 10500 Å, depending on the grism or volume-phased holographic gratings (VPHs) used (see Table 2.4 for details).

2.2.1.4 TNG/DOLORES

Another telescope that is used for the followup of the sources is the Telescopio Galileo Galilei (TNG), a 3.58 m optical telescope placed at the Roque de los Muchachos Observatory on the island of La Palma, Spain. TNG is operated by the 'Fundacion Galileo Galilei, with is financed by the Istituto Nazionale di Astrofisica (INAF)

For the long slit spectroscopy, we used the Device Optimized for the LOw RESolution (DOLORES, or LRS), that is placed at the at one of the Nasmyth focus of the TNG. This instrument provides low resolution spectroscopy with R=600-6000, depending on the grism used (details of each grism are shown in Table 2.5). With LRS we can acquire spectrum in the wavelength range of from 3000 to 10073 Å. The detector have a field of view of 8.6' $\times$ 8.6'. The slits available have widths between 0.7" and 5.0".

TABLE 2.5: TNG/DOLORES setup for long slit spectroscopy.

Name	Disp . (Å/pix)	λ_{min} (Å)	λ_c (Å)	λ_{max} (Å)	R (for 1" slit)
LR-B	2.52	3000	5850	8430	585
LR-R	2.61	4470	7400	10073	714
V390	0.26	3634	3900	4166	3766
V486	0.20	4612	4725	4838	5953
V510	0.22	4875	5100	5325	5950
V589	0.27	5619	5895	6171	5502
V656	0.32	6232	6560	6888	5248
V860	0.44	8149	8600	9051	4000
VHRV	0.95	4752	5725	6698	1527
VHRR	0.70	6238	7000	7717	2513
VHRI	0.68	7433	8130	8826	3035

TABLE 2.6: WHT/ISIS blue arm setup for long slit spectroscopy.

Grating	Blaze	Spectral range (Å)	Dispersion (Å/pix)	Resol. with a 1" slit (Å)	R
R158B	3600	6635	1.62	7.81	512
R300B	4000	3539	0.86	4.1	976
R600B	3900	1825	0.45	2.02	1980
R1200B	4000	940	0.23	0.85	4706
H2400B	Holo	442	0.11	0.35	11429

2.2.1.5 WHT/ISIS

Other telescope that is used in this thesis is the 4.2 m William Herschel Telescope (WHT), that is part of the Isaac Newton Group of Telescopes (ING) situated at the Roque de los Muchachos Observatory at La Palma island, Spain. The ING is operated by the Particle Physics And Astronomy Research Council (PPARC) of the United Kingdom, the Nederlandse Organisatie voor Wetenschappelijk Onderzoek (NWO) of the Netherlands and the Instituto de Astrofísica de Canarias (IAC) of Spain.

Spectroscopy with the WHT is conducted using the Intermediate dispersion Spectrograph and Imaging System (ISIS), mounted at the Cassegrain focus. The instrument consists on two arms, so a dichroic divides the incoming light in two beams with the dividing wavelength at roughly 5300 Å. The blue arm works with a wavelength range between 3000 and 6000 Å, and the red arm between 5000 and 10000 Å. The spectral resolutions are between R=500 and R=12000 for the blue arm, and between R=900 and R=10000 for the red arm (see Table 2.6 and Table 2.7 for details for each arm). ISIS uses slits with a length of 4' and widths between 0.14" and 22.6".

TABLE 2.7: WHT/ISIS red arm setup for long slit spectroscopy.

Grating	Blaze	Spectral range (Å)	Dispersion (Å/pix)	Resol. with a 1" slit (Å)	R
R158R	6500	7530	1.81	7.7	909
R316R	6500	3858	0.93	3.8	1842
R600R	7000	2054	0.49	1.81	3867
R1200R	7200	1055	0.26	0.75	9333

TABLE 2.8: R for WHT/ACAM long slit spectroscopy calculated with different slit widths.

Wavelength	0.75 ''	1.0 ''	1.25 ''
3800 Å	390	290	230
5650 Å	580	430	350
7500 Å	770	570	460

2.2.1.6 WHT/ACAM

With the WHT, we use other instrument for spectroscopy, that is the auxiliary-port camera ACAM. This instrument is mounted at a Cassegrain focus and can be used not only for low resolution spectroscopy, but for broad-band imaging, narrow-band imaging as well. ACAM works with a spectral range of 3500-9400 Å. The dispersor is a VPH grating, modelled to deliver the spectral resolution R on axis (this is, with the target near the middle of the slit) that is shown in Table 2.8. ACAM have slit widths between 0.5" and 10".

2.2.1.7 NOT/ALFOSC

The 2.5 m Nordic Optical Telescope (NOT) is used for optical follow up. It is located at Roque de los Muchachos, La Palma, Canarias, Spain, and was constructed and is operated by the Nordic Optical Telescope Scientific Association (NOTSA).

The instrument used to obtain the spectra is the Andalucia Faint Object Spectrograph and Camera (ALFOSC). The instrument have horizontal slits with widths ranging from 0.4" to 40.0'' and 6.3' length (except the 1.0" and 1.8" slits, that have a length of 5.3'), and vertical long slits with widths from 0.5" to 10.0" and a length of 5.3'. The dispersor elements are listed in Table 2.9.

2.2.1.8 NTT/EFOSC2

Other telescope used from the observatory at La Silla, at an altitude of 2400 metre in the southern part of the chilean Atacama desert, is the ESO New Technology Telescope (NTT), that is an altitude-azimuth Richey-Chretien telescope with a diameter of its primary mirror of 3.58 m.

TABLE 2.9: NOT/ALFOSC setup for long slit spectroscopy.

Grism	Grating (rules/mm)	λ_{blaze} (Å)	λ_c (Å)	Dispersion (Å)	R (for 1" slit)
3	400	3900	4320	2.3	350
4	300	4800	5800	3.3	360
5	300	6500	7000	3.5	415
6	600	3900	4020	1.5	490
7	600	5300	5260	1.7	650
8	600	6500	7030	1.4	1000
10	150	3800	3870	5.9	105
11	200	5200	5000	4.6	190
12	75	7300	6930	12	95
14	600	4288	4630	1.6	600
16	1000	4069	4280	0.86	1000
17	2400 VPH	-	6580	0.26	5000
18	1086 VPH	-	4360	0.93	1000
19	823 VPH	-	5640	1.2	970
20	484 VPH	-	7850	2.2	770

We use the ESO Faint Object Spectrograph and Camera v.2 (EFOSC2) to obtain low resolution spectroscopy for the optical followup of the sources. This telescope have a great variety of grisms, with wavelength ranges from 3200 to 11000 Å. The resolution varies from R=600 to R=14000, as seen in Table 2.10.

2.2.2 Fiber spectra from SDSS survey

In order to identify the optical counterparts of the X-ray sources, we use as well the public spectra from the Sloan Digital Sky Survey (SDSS) until the Data Release 14 (Abolfathi *et al.* 2018). The SDSS is an international collaboration that uses a dedicated 2.5m modified Ritchey-Chrétien altitude-azimuth telescope placed at the Apache Point Observatory, New Mexico, USA, at 2788 m above the sea level.

The telescope can work on imaging and spectroscopic mode. To do so, the camera at the Cassegrain focus must be changed to the corresponding instrument. To obtain optical spectra, SDSS uses plates that are drilled specifically to observe the chosen celestial objects of interest for each sky field observed. Each hole in the plate is connected a fiber to drive the incoming radiation to the two spectrographs mounted on the image rotator.

For this thesis we use the data collected using two different spectrographs, the old SDSS-I/II spectrograph and the most modern one, the Baryon Oscillation Spectroscopic Survey (BOSS) spectrograph. In Fig. 2.4 we show a sketch of the instrument.

Table 2.10: NTT/EFOSC2 setup for long slit spectroscopy.

Grisms	Wavelength range	Grating (gr/mm)	Blaze angle (Å)	Dispersion (Å/pix)	R	Resolution FWHM (Å)
Gr 01	3185-10940	100	4500	6.66	676	48.0
Gr 02	5100-11000	100	6700	6.6	1015	49.6
Gr 03	3050-6100	400	3900	1.5	2600	11.6
Gr 04	4085-7520	360	4700	1.68	2798	12.6
Gr 05	5200-9350	300	6700	2.06	3252	15.4
Gr 06	3860-8070	300	5000	2.06	2427	15.5
Gr 07	3270-5240	600	3800	0.96	3958	7.4
Gr 08	4320-6360	600	5300	0.99	5354	7.4
Gr 09	4700-6770	600	5600	1.0	5600	7.6
Gr 10	6280-8200	600	6500	0.95	6842	7.1
Gr 11	3380-7520	300	4000	2.04	1961	15.8
Gr 12	6015-10320	300	7900	2.12	3726	16.0
Gr 13	3685-9315	236	4400	2.77	1588	21.2
Gr 14	3095-5085	600	4000	0.93	4301	7.0
Gr 15	6895-8765	600	8300	0.86	9651	6.5
Gr 16	6015-10320	300	7900	2.12	3726	16.0
Gr 17	6895-8765	600	8300	0.92	9022	6.5
Gr 18	4700-6770	600	5600	1.0	5600	7.6
Gr 19	4441-5114	1557	4777	0.34	14050	1.5
Gr 20	6047-7147	1070	6597	0.55	11995	2.0

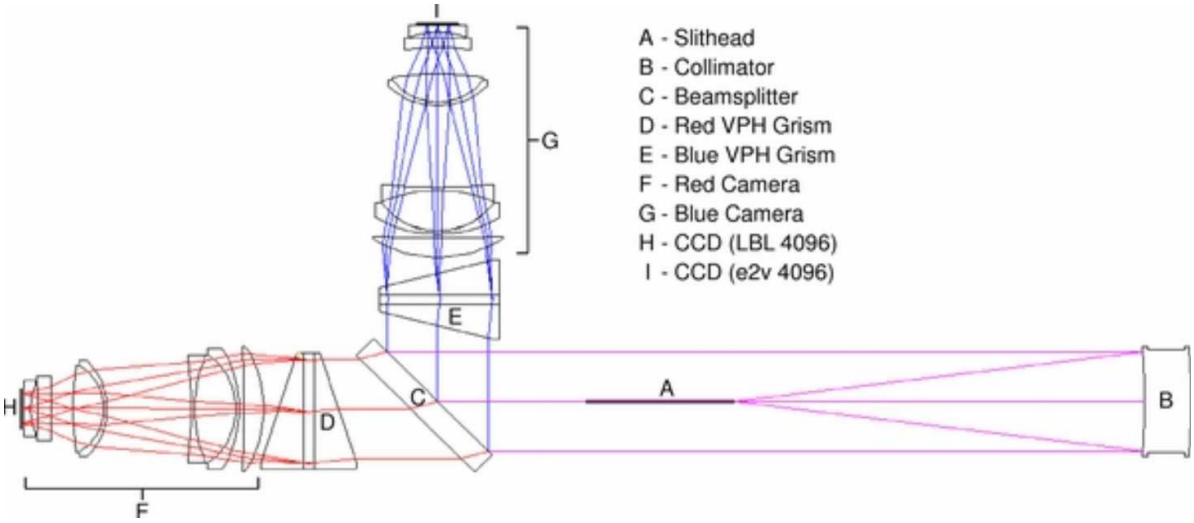

Figure 2.4: Diagram of the BOSS instrument (credit: ESA).

2.2.2.1 SDSS-I/II Spectrograph

The first spectroscopic instrument from SDSS acquired spectra from 640 positions in the sky for each aluminium plate. The optical fibers carry the incoming light from the focal plane to slitheads attached to the cartridge. The light is driven to two spectrographs one to cover the blue wavelength range of 3800 to 6100 Å and the other for the red part of the spectra, from 5900 to 9100 Å. The beam is splitted with a dichroic with the dividing wavelength at around 6000 Å. Each spectrograph collects the radiation with one SITe/Tektronix 2048 $\times$ 2048 CCD for each arm. This setup allows to have a resolution ranging from 1850 to 2200 for the spectral range of 3900-9100 Å.

2.2.2.2 BOSS Spectrograph

The BOSS spectrograph were a redesign of the originals SDSS spectrographs and were rebuilt from them. In this case, the aluminium plates are drilled with 1000 holes corresponding to a determinate position in the sky, and the fibers have a diameter of 2". The new instrument can provide a spectra with a wavelength range of 3600-10400 Å. The light for each object is splitted with a dichroic at roughly 6000 Å. The light is then carried to two arms, the blue channel has a wavelength range of 3700-6000 Å with an spectral resolution ranging from R=1560 to R=2270, at 3700 and 6000 Å, respectively. The red arm have a resolution ranging from R=1850 to R=2650, at 6000 and 9000, respectively.

Chapter 3

The BUXS Sample

- SEDs

3.1 Sample definition

In this section we explain how the BUXS sample is selected and the final selection, optical completeness.

3.2 X-ray modeling

In this section we explain how the X-ray data were treated. We explain that we combine all the available observations. After that sources were extracted using info from other part. Apart from that we explain that the spectral modelig were based on XMMFITCAT. This is how we select the best model, how we calculate the parameters as the luminosity and nh and how compute errors.

3.3 Optical spectral continuum modeling

In this section we explain the reduction of an optical spectrum. We may distinguish between echelle of xshooter and long slit spectra from other telescopes, as one was analyzed with STARLIGHT and power laws, and the other with SHERPA and combinations of templates.

Apart from that we explain the ways of fitting the optical spectra. We talk about STARLIGHT for the xshooter, and sherpa for the BUXS sample.

The general model is AGN plus SMC extinction and additive host galaxy model. For some objects where we have data in the high order f the Balmer lines and higher, it is necessary to introduce FeII and Balmer Continuum emission, so we describe all the components here.

3.4 Optical emision lines fits

Here we describe the H_α, H_β and MgII line fit models. The NLR uses the same width in velocity. We use the FWHM and flux as free parameters.

3.5 Subsample used in this thesis

Here we give details of the data used in this thesis. In the following chapters we explain more precisely the subsamples.

Chapter 4

Detailed modeling of two sources

This chapter is about the two discordant AGN observed with XSHOOTER. We re-format the article to show the results and possible origin of the discordance.

4.1 Subsample of two objects

We describe here the two objects selected with XSHOOTER

4.2 X-ray properties

Here we explain the X-ray spectral fitting of the two sources.

4.3 UV-to NIR observations

In this section we describe the observations from the VLT.

4.4 Analysis and results

4.4.1 AGN and host galaxy continuum decomposition

With STARLIGHT we decompose the extracted spectrum and divide it into host galaxy and AGN emission, with the STARLIGHT software.

4.4.2 Narrow and broad line Balmer decrements

After removing the host galaxy contamination, we fit the emission lines.

4.4.3 SMBH masses

Using the broad H_α line, we obtain the SMBH masses of each AGN.

4.4.4 Host galaxy masses

4.4.4.1 Stellar masses

We obtain the host galaxy stellar mass from the STARLIGHT software

4.4.4.2 Dynamical masses

From the NaID, we estimate the host galaxy dynamical masses, and compare it with the stellar masses.

4.5 Discussion

Here we describe the possible causes of the discordance between the optical and X-ray classifications.

4.5.1 Compton-thick or Compton-thin obscuration

Using line flux ratios, we determine that the sources are not Compton-thick AGN.

4.5.2 Host dilution

We compare the SMBH and the host galaxy masses to check if the host galaxy is more massive than expected through the SMBH and the host galaxy relations.

4.5.3 Dust-to-gas ratio ot the obscuring medium

We check if the obscuring medium is more dusty than the Galactic dust-to-gas relation.

4.5.4 Intrinsically weak BLR region

To check if the broad lines are underluminous and that is why they are hard to detect.

4.5.5 Variability

We explain the possible impact of variability in the sources.

4.6 Results

We point out that one source have higher dust-to-gas ratio than the Galactic, and other is hosted by a massive galaxy.

Chapter 5

Analysis of BUXS sample

We study the obscuration of type-1 AGN by comparing the optical extinction and the X-ray absorption.

5.1 Sample definition

We describe here that we select all objects that show at least one broad line in their optical spectrum, that is ranging from type-1.0 to type-1.8/9, often grouped with type-2 AGN. We use only the redshift range of z=0.05-1 to measure in a robust way the X-ray obscuration.

5.2 X-ray and optical

5.2.1 X-ray properties

Here we explain the X-ray spectral fitting of the type-1 sources. In this section we also examine the percentage of X-ray absorbed sources and compare it with other samples. We test the evolution of the X-ray luminosity with the fraction of absorbed sources.

5.2.2 Optical spectrum fits

We describe the model used to fit the optical spectrum. This allows us to measure the optical extinction of the sources in terms of Av. We can compare here the Av range of other selections and the fraction of sources not optically obscured.

5.2.2.1 SED Av vs spectrum Av

We compare this estimations with the ones from the SED analysis.

5.2.2.2 Balmer decrement Av vs spectrum Av

We compare this estimations with the ones where H_α and H_β are available. We test if there is an intrinsic H_α/H_β ratio, or it depends on the conditions on the BLR.

5.3 Subdivision in Seyfert subclases

We study the change in parameters such as Av, NH, etc with the Seyfert subclass. We also check with different redshifts if there is an evolution or not.

5.4 Optical extinction versus X-ray absorption

We plot the Av vs NH, and we compute the fraction of sources that follows the Galactic dust-to-gas relation, the ones that are more dusty and the ones that have more gas.

5.5 Dust-to-gas ratio

Plotting the dust-to-gas ratio versus the luminosity or redshift to test if there is any dependence in between those quantities.

5.6 Bolometric luminosity and Bolometric correction

Here we test if the relations between the Bolometric luminosity based on the optical spectrum and the luminosity of the X-rays is compatible with the ones reported in other studies.

5.7 Conclusions of the statistical study

We summarize the main differences that this complete sample of type-1 AGN have with other optical or X-ray selected samples. We explain this differences with context with the unified model of AGN and with the latest explanations in the literature of optical extinction and X-ray absorption.

Chapter 6

Conclusions and future work

6.1 Conclusions of this thesis

6.1.1 Detailed analysis of two X-ray unabsorbed type-2 objects

We determined that the discordant optical and X-ray sources are not a physical family, as the origin of the discordance can be very different.

6.1.2 Optical extinction and X-ray absorption of a complete type-1 sample

The preliminar results obtained is that using a complete sample of X-ray selected type-1 AGN at hard energies we can detect objects with high levels of obscuration in the optical and in the X-rays. The majority of the sources follow the Galactic relation, but there are a significant fraction of discordant sources.

6.2 Future work

Here we explain possible studies that can be derived from this work, that could not be studied in this thesis.

Appendix A

Tables

Along this appendix a table is presented

References

Abazajian, K.N., Adelman-McCarthy, J.K., Agüeros, M.A., Allam, S.S., Allende Prieto, C., An, D., Anderson, K.S.J., Anderson, S.F., Annis, J., Bahcall, N.A., Bailer-Jones, C.A.L., Barentine, J.C., Bassett, B.A., Becker, A.C., Beers, T.C., Bell, E.F., Belokurov, V., Berlind, A.A., Berman, E.F., Bernardi, M., Bickerton, S.J., Bizyaev, D., Blakeslee, J.P., Blanton, M.R., Bochanski, J.J., Boroski, W.N., Brewington, H.J., Brinchmann, J., Brinkmann, J., Brunner, R.J., Budavári, T., Carey, L.N., Carliles, S., Carr, M.A., Castander, F.J., Cinabro, D., Connolly, A.J., Csabai, I., Cunha, C.E., Czarapata, P.C., Davenport, J.R.A., de Haas, E., Dilday, B., Doi, M., Eisenstein, D.J., Evans, M.L., Evans, N.W., Fan, X., Friedman, S.D., Frieman, J.A., Fukugita, M., Gänsicke, B.T., Gates, E., Gillespie, B., Gilmore, G., Gonzalez, B., Gonzalez, C.F., Grebel, E.K., Gunn, J.E., György, Z., Hall, P.B., Harding, P., Harris, F.H., Harvanek, M., Hawley, S.L., Hayes, J.J.E., Heckman, T.M., Hendry, J.S., Hennessy, G.S., Hindsley, R.B., Hoblitt, J., Hogan, C.J., Hogg, D.W., Holtzman, J.A., Hyde, J.B., Ichikawa, S.-i., Ichikawa, T., Im, M., Ivezić, Ž., Jester, S., Jiang, L., Johnson, J.A., Jorgensen, A.M., Jurić, M., Kent, S.M., Kessler, R., Kleinman, S.J., Knapp, G.R., Konishi, K., Kron, R.G., Krzesinski, J., Kuropatkin, N., Lampeitl, H., Lebedeva, S., Lee, M.G., Lee, Y.S., French Leger, R., Lépine, S., Li, N., Lima, M., Lin, H., Long, D.C., Loomis, C.P., Loveday, J., Lupton, R.H., Magnier, E., Malanushenko, O., Malanushenko, V., Mandelbaum, R., Margon, B., Marriner, J.P., Martínez-Delgado, D., Matsubara, T., McGehee, P.M., McKay, T.A., Meiksin, A., Morrison, H.L., Mullally, F., Munn, J.A., Murphy, T., Nash, T., Nebot, A., Neilsen, E.H., Jr., Newberg, H.J., Newman, P.R., Nichol, R.C., Nicinski, T., Nieto-Santisteban, M., Nitta, A., Okamura, S., Oravetz, D.J., Ostriker, J.P., Owen, R., Padmanabhan, N., Pan, K., Park, C., Pauls, G., Peoples, J., Jr., Percival, W.J., Pier, J.R., Pope, A.C., Pourbaix, D., Price, P.A., Purger, N., Quinn, T., Raddick, M.J., Re Fiorentin, P., Richards, G.T., Richmond, M.W., Riess, A.G., Rix, H.-W., Rockosi, C.M., Sako, M., Schlegel, D.J., Schneider, D.P., Scholz, R.-D., Schreiber, M.R., Schwope, A.D., Seljak, U., Sesar, B., Sheldon, E., Shimasaku, K., Sibley, V.C., Simmons, A.E., Sivarani, T., Allyn Smith, J., Smith, M.C., Smolčić, V., Snedden, S.A., Stebbins, A., Steinmetz, M., Stoughton, C., Strauss, M.A., SubbaRao, M., Suto, Y., Szalay, A.S., Szapudi, I., Szkody, P., Tanaka, M., Tegmark, M., Teodoro, L.F.A., Thakar, A.R., Tremonti, C.A., Tucker, D.L., Uomoto, A., Vanden Berk, D.E., Vandenberg, J., Vidrih, S., Vogeley, M.S., Voges, W., Vogt, N.P., Wadadekar, Y., Watters, S., Weinberg, D.H., West, A.A., White, S.D.M., Wilhite, B.C., Wonders, A.C., Yanny, B., Yocum, D.R., York, D.G., Zehavi, I., Zibetti, S., and Zucker, D.B.: 2009, *The Astrophysical Journal Supplement Series* **182**, 543-558.

Abolfathi, B., Aguado, D.S., Aguilar, G., Allende Prieto, C., Almeida, A., Tasnim Ananna, T., Anders, F., Anderson, S.F., Andrews, B.H., Anguiano, B., Aragón-Salamanca, A., Argudo-Fernández, M., Armengaud, E., Ata, M., Aubourg, E., Avila-Reese, V., Badenes, C., Bailey, S., Balland, C., Barger, K.A., Barrera-Ballesteros, J., Bartosz, C., Bastien, F., Bates, D., Baumgarten, F., Bautista, J., Beaton, R., Beers, T.C., Belfiore, F., Bender, C.F., Bernardi, M., Bershady, M.A., Beutler, F., Bird, J.C., Bizyaev, D., Blanc, G.A.,

Blanton, M.R., Blomqvist, M., Bolton, A.S., Boquien, M., Borissova, J., Bovy, J., Andres Bradna Diaz, C., Nielsen Brandt, W., Brinkmann, J., Brownstein, J.R., Bundy, K., Burgasser, A.J., Burtin, E., Busca, N.G., Cañas, C.I., Cano-Díaz, M., Cappellari, M., Carrera, R., Casey, A.R., Cervantes Sodi, B., Chen, Y., Cherinka, B., Chiappini, C., Doohyun Choi, P., Chojnowski, D., Chuang, C.-H., Chung, H., Clerc, N., Cohen, R.E., Comerford, J.M., Comparat, J., Correa do Nascimento, J., da Costa, L., Cousinou, M.-C., Covey, K., Crane, J.D., Cruz-Gonzalez, I., Cunha, K., da Silva Ilha, G., Damke, G.J., Darling, J., Davidson, J.W., Jr., Dawson, K., de Icaza Lizaola, M.A.C., de la Macorra, A., de la Torre, S., De Lee, N., de Sainte Agathe, V., Deconto Machado, A., Dell'Agli, F., Delubac, T., Diamond-Stanic, A.M., Donor, J., José Downes, J., Drory, N., du Mas des Bourboux, H., Duckworth, C.J., Dwelly, T., Dyer, J., Ebelke, G., Davis Eigenbrot, A., Eisenstein, D.J., Elsworth, Y.P., Emsellem, E., Eracleous, M., Erfanianfar, G., Escoffier, S., Fan, X., Fernández Alvar, E., Fernandez-Trincado, J.G., Cirolini, R.F., Feuillet, D., Finoguenov, A., Fleming, S.W., Font-Ribera, A., Freischlad, G., Frinchaboy, P., Fu, H., Gómez Maqueo Chew, Y., Galbany, L., García Pérez, A.E., Garcia-Dias, R., García-Hernández, D.A., Garma Oehmichen, L.A., Gaulme, P., Gelfand, J., Gil-Marín, H., Gillespie, B.A., Goddard, D., González Hernández, J.I., Gonzalez-Perez, V., Grabowski, K., Green, P.J., Grier, C.J., Gueguen, A., Guo, H., Guy, J., Hagen, A., Hall, P., Harding, P., Hasselquist, S., Hawley, S., Hayes, C.R., Hearty, F., Hekker, S., Hernandez, J., Hernandez Toledo, H., Hogg, D.W., Holley-Bockelmann, K., Holtzman, J.A., Hou, J., Hsieh, B.-C., Hunt, J.A.S., Hutchinson, T.A., Hwang, H.S., Jimenez Angel, C.E., Johnson, J.A., Jones, A., Jönsson, H., Jullo, E., Sakil Khan, F., Kinemuchi, K., Kirkby, D., Kirkpatrick, C.C., IV, Kitaura, F.-S., Knapp, G.R., Kneib, J.-P., Kollmeier, J.A., Lacerna, I., Lane, R.R., Lang, D., Law, D.R., Le Goff, J.-M., Lee, Y.-B., Li, H., Li, C., Lian, J., Liang, Y., Lima, M., Lin, L., Long, D., Lucatello, S., Lundgren, B., Mackereth, J.T., MacLeod, C.L., Mahadevan, S., Geimba Maia, M.A., Majewski, S., Manchado, A., Maraston, C., Mariappan, V., Marques-Chaves, R., Masseron, T., Masters, K.L., McDermid, R.M., McGreer, I.D., Melendez, M., Meneses-Goytia, S., Merloni, A., Merrifield, M.R., Meszaros, S., Meza, A., Minchev, I., Minniti, D., Mueller, E.-M., Muller-Sanchez, F., Muna, D., Muñoz, R.R., Myers, A.D., Nair, P., Nandra, K., Ness, M., Newman, J.A., Nichol, R.C., Nidever, D.L., Nitschelm, C., Noterdaeme, P., O'Connell, J., Oelkers, R.J., Oravetz, A., Oravetz, D., Aquino Ortíz, E., Osorio, Y., Pace, Z., Padilla, N., Palanque-Delabrouille, N., Alonso Palicio, P., Pan, H.-A., Pan, K., Parikh, T., Pâris, I., Park, C., Peirani, S., Pellejero-Ibanez, M., Penny, S., Percival, W.J., Perez-Fournon, I., Petitjean, P., Pieri, M.M., Pinsonneault, M., Pisani, A., Prada, F., Prakash, A., Queiroz, A.B.d.A., Raddick, M.J., Raichoor, A., Barboza Rembold, S., Richstein, H., Riffel, R.A., Riffel, R., Rix, H.-W., Robin, A.C., Rodríguez Torres, S., Román-Zúñiga, C., Ross, A.J., Rossi, G., Ruan, J., Ruggeri, R., Ruiz, J., Salvato, M., Sánchez, A.G., Sánchez, S.F., Sanchez Almeida, J., Sánchez-Gallego, J.R., Santana Rojas, F.A., Santiago, B.X., Schiavon, R.P., Schimoia, J.S., Schlafly, E., Schlegel, D., Schneider, D.P., Schuster, W.J., Schwope, A., Seo, H.-J., Serenelli, A., Shen, S., Shen, Y., Shetrone, M., Shull, M., Silva Aguirre, V., Simon, J.D., Skrutskie, M., Slosar, A., Smethurst, R., Smith, V., Sobeck, J., Somers, G., Souter, B.J., Souto, D., Spindler, A., Stark, D.V., Stassun, K., Steinmetz, M., Stello, D., Storchi-Bergmann, T., Streblyanska, A., Stringfellow, G.S., Suárez, G., Sun, J., Szigeti, L., Taghizadeh-Popp, M., Talbot, M.S., Tang, B., Tao, C., Tayar, J., Tembe, M., Teske, J., Thakar, A.R., Thomas, D., Tissera, P., Tojeiro, R., Tremonti, C., Troup, N.W., Urry, M., Valenzuela, O., van den Bosch, R., Vargas-González, J., Vargas-Magaña, M., Vazquez, J.A., Villanova, S., Vogt, N., Wake, D., Wang, Y., Weaver, B.A., Weijmans, A.-M., Weinberg, D.H., Westfall, K.B., Whelan, D.G., Wilcots, E., Wild, V., Williams, R.A., Wilson, J., Wood-Vasey, W.M., Wylezalek, D., Xiao, T., Yan, R., Yang, M., Ybarra, J.E., Yèche, C., Zakamska, N., Zamora, O., Zarrouk, P., Zasowski, G., Zhang, K., Zhao, C., Zhao, G.-B., Zheng, Z., Zheng, Z., Zhou, Z.-M., Zhu, G., Zinn, J.C., and Zou, H.: 2018, *The Astrophysical Journal Supplement Series* **235**, 42.

Akylas, A. and Georgantopoulos, I.: 2009, *Astron. Astroph.* **500**, 999.

Allen, C.W.: 1973, *London: University of London, Athlone Press, —c1973, 3rd ed.*.

Antonucci, R.: 1993, *Annual Review of Astronomy and Astrophysics* **31**, 473.

Arnaud, K.A.: 1996, *Astronomical Data Analysis Software and Systems V* **101**, 17.

Asmus, D., Gandhi, P., Smette, A., Hönig, S.F., and Duschl, W.J.: 2011, *Astron. Astroph.* **536**, A36.

Barcons, X., Carrera, F.J., and Ceballos, M.T.: 2003, *Monthly Notices of the Royal Astronomical Society* **339**, 757.

Baron, D., Stern, J., Poznanski, D., and Netzer, H.: 2016, *Astrophys. J.* **832**, 8.

Bassani, L., Dadina, M., Maiolino, R., Salvati, M., Risaliti, G., Della Ceca, R., Matt, G., and Zamorani, G.: 1999, *The Astrophysical Journal Supplement Series* **121**, 473.

Bell, E.F. and de Jong, R.S.: 2001, *Astrophys. J.* **550**, 212.

Bianchi, S., Corral, A., Panessa, F., Barcons, X., Matt, G., Bassani, L., Carrera, F.J., and Jiménez-Bailón, E.: 2008, *Monthly Notices of the Royal Astronomical Society* **385**, 195.

Bianchi, S., Panessa, F., Barcons, X., Carrera, F.J., La Franca, F., Matt, G., Onori, F., Wolter, A., Corral, A., Monaco, L., Ruiz, Á., and Brightman, M.: 2012, *Monthly Notices of the Royal Astronomical Society* **426**, 3225.

Braito, V., Franceschini, A., Della Ceca, R., Severgnini, P., Bassani, L., Cappi, M., Malaguti, G., Palumbo, G.G.C., Persic, M., Risaliti, G., and Salvati, M.: 2003, *Astron. Astroph.* **398**, 107.

Braito, V., Reeves, J.N., Sambruna, R.M., and Gofford, J.: 2011, *Monthly Notices of the Royal Astronomical Society* **414**, 2739.

Brightman, M., Nandra, K., Salvato, M., Hsu, L.-T., Aird, J., and Rangel, C.: 2014, *Monthly Notices of the Royal Astronomical Society* **443**, 1999.

Bruzual, G. and Charlot, S.: 2003, *Monthly Notices of the Royal Astronomical Society* **344**, 1000.

Burtscher, L., Davies, R.I., Graciá-Carpio, J., Koss, M.J., Lin, M.-Y., Lutz, D., Nandra, P., Netzer, H., Orban de Xivry, G., Ricci, C., Rosario, D.J., Veilleux, S., Contursi, A., Genzel, R., Schnorr-Müller, A., Sternberg, A., Sturm, E., and Tacconi, L.J.: 2016, *Astron. Astroph.* **586**, A28.

Caccianiga, A., Severgnini, P., Braito, V., Della Ceca, R., Maccacaro, T., Wolter, A., Barcons, X., Carrera, F.J., Lehmann, I., Page, M.J., Saxton, R., and Webb, N.A.: 2004, *Astron. Astroph.* **416**, 901.

Caccianiga, A., Severgnini, P., Della Ceca, R., Maccacaro, T., Carrera, F.J., and Page, M.J.: 2007, *Astron. Astroph.* **470**, 557.

Caccianiga, A., Severgnini, P., Della Ceca, R., Maccacaro, T., Cocchia, F., Barcons, X., Carrera, F.J., Matute, I., McMahon, R.G., Page, M.J., Pietsch, W., Sbarufatti, B., Schwope, A., Tedds, J.A., and Watson, M.G.: 2008, *Astron. Astroph.* **477**, 735.

Calzetti, D., Armus, L., Bohlin, R.C., Kinney, A.L., Koornneef, J., and Storchi-Bergmann, T.: 2000, *Astrophys. J.* **533**, 682.

Cappellari, M., Bacon, R., Bureau, M., Damen, M.C., Davies, R.L., de Zeeuw, P.T., Emsellem, E., Falcón-Barroso, J., Krajnović, D., Kuntschner, H., McDermid, R.M., Peletier, R.F., Sarzi, M., van den Bosch, R.C.E., and van de Ven, G.: 2006, *Monthly Notices of the Royal Astronomical Society* **366**, 1126.

Cardelli, J.A., Clayton, G.C., and Mathis, J.S.: 1989, *Astrophys. J.* **345**, 245.

Carrera, F.J., Page, M.J., and Mittaz, J.P.D.: 2004, *Astron. Astroph.* **420**, 163.

Cid Fernandes, R., Mateus, A., Sodré, L., Stasińska, G., and Gomes, J.M.: 2005, *Monthly Notices of the Royal Astronomical Society* **358**, 363.

Comastri, A.: 2004, *Supermassive Black Holes in the Distant Universe* **308**, 245.

Comastri, A., Setti, G., Zamorani, G., and Hasinger, G.: 1995, *Astron. Astroph.* **296**, 1.

Corral, A., Barcons, X., Carrera, F.J., Ceballos, M.T., and Mateos, S.: 2005, *Astron. Astroph.* **431**, 97.

Corral, A., Della Ceca, R., Caccianiga, A., Severgnini, P., Brunner, H., Carrera, F.J., Page, M.J., and Schwope, A.D.: 2011, *Astron. Astroph.* **530**, A42.

Corral, A., Georgantopoulos, I., Watson, M.G., Rosen, S.R., Page, K.L., and Webb, N.A.: 2015, *Astron. Astroph.* **576**, A61.

Crenshaw, D.M.: 1986, *The Astrophysical Journal Supplement Series* **62**, 821.

Del Moro, A., Alexander, D.M., Bauer, F.E., Daddi, E., Kocevski, D.D., McIntosh, D.H., Stanley, F., Brandt, W.N., Elbaz, D., Harrison, C.M., Luo, B., Mullaney, J.R., and Xue, Y.Q.: 2016, *Monthly Notices of the Royal Astronomical Society* **456**, 2105.

den Herder, J.W., Brinkman, A.C., Kahn, S.M., Branduardi-Raymont, G., Thomsen, K., Aarts, H., Audard, M., Bixler, J.V., den Boggende, A.J., Cottam, J., Decker, T., Dubbeldam, L., Erd, C., Goulooze, H., Güdel, M., Guttridge, P., Hailey, C.J., Janabi, K.A., Kaastra, J.S., de Korte, P.A.J., van Leeuwen, B.J., Mauche, C., McCalden, A.J., Mewe, R., Naber, A., Paerels, F.B., Peterson, J.R., Rasmussen, A.P., Rees, K., Sakelliou, I., Sako, M., Spodek, J., Stern, M., Tamura, T., Tandy, J., de Vries, C.P., Welch, S., and Zehnder, A.: 2001, *Astron. Astroph.* **365**, L7.

Della Ceca, R., Pellegrini, S., Bassani, L., Beckmann, V., Cappi, M., Palumbo, G.G.C., Trinchieri, G., and Wolter, A.: 2001, *Astron. Astroph.* **375**, 781.

Dickey, J.M. and Lockman, F.J.: 1990, *Annual Review of Astronomy and Astrophysics* **28**, 215.

Ferguson, J.W., Korista, K.T., and Ferland, G.J.: 1997, *The Astrophysical Journal Supplement Series* **110**, 287.

Ferrarese, L. and Merritt, D.: 2000, *Astrophys. J.* **539**, L9.

Freeman, P., Doe, S., and Siemiginowska, A.: 2001, in J. L. Starck & F. D. Murtagh (ed.), *Society of Photo-Optical Instrumentation Engineers (SPIE) Conference Series*, Vol. 4477 of *Presented at the Society of Photo-Optical Instrumentation Engineers (SPIE) Conference*, pp 76–87

Fruscione, A., McDowell, J. C., Allen, G. E., Brickhouse, N. S., Burke, D. J., Davis, J. E., Durham, N., Elvis, M., Galle, E. C., Harris, D. E., Huenemoerder, D. P., Houck, J. C., Ishibashi, B., Karovska, M., Nicastro, F., Noble, M. S., Nowak, M. A., Primini, F. A., Siemiginowska, A., Smith, R. K., and Wise, M.: 2006, in *Society of Photo-Optical Instrumentation Engineers (SPIE) Conference Series*, Vol. 6270 of *Presented at the Society of Photo-Optical Instrumentation Engineers (SPIE) Conference*

Galbiati, E., Caccianiga, A., Maccacaro, T., Braito, V., Della Ceca, R., Severgnini, P., Brunner, H., Lehmann, I., and Page, M.J.: 2005, *Astron. Astroph.* **430**, 927.

Gandhi, P., Horst, H., Smette, A., Hönig, S., Comastri, A., Gilli, R., Vignali, C., and Duschl, W.: 2009, *Astron. Astroph.* **502**, 457.

Gandhi, P., Lansbury, G.B., Alexander, D.M., Stern, D., Arévalo, P., Ballantyne, D.R., Baloković, M., Bauer, F.E., Boggs, S.E., Brandt, W.N., Brightman, M., Christensen, F.E., Comastri, A., Craig, W.W., Del Moro, A., Elvis, M., Fabian, A.C., Hailey, C.J., Harrison, F.A., Hickox, R.C., Koss, M., LaMassa, S.M., Luo, B., Madejski, G.M., Ptak, A.F., Puccetti, S., Teng, S.H., Urry, C.M., Walton, D.J., and Zhang, W.W.: 2014, *Astrophys. J.* **792**, 117.

García-González, J., Alonso-Herrero, A., Pérez-González, P.G., Hernán-Caballero, A., Sarajedini, V.L., and Villar, V.: 2015, *Monthly Notices of the Royal Astronomical Society* **446**, 3199.

Gaskell, C.M. and Goosmann, R.W.: 2013, *Astrophys. J.* **769**, 30.

Gebhardt, K., Bender, R., Bower, G., Dressler, A., Faber, S.M., Filippenko, A.V., Green, R., Grillmair, C., Ho, L.C., Kormendy, J., Lauer, T.R., Magorrian, J., Pinkney, J., Richstone, D., and Tremaine, S.: 2000, *Astrophys. J.* **539**, L13.

Georgantopoulos, I. and Georgakakis, A.: 2005, *Monthly Notices of the Royal Astronomical Society* **358**, 131.

Georgantopoulos, I., Rovilos, E., Xilouris, E.M., Comastri, A., and Akylas, A.: 2011, *Astron. Astroph.* **526**, A86.

Georgantopoulos, I., Rovilos, E., Akylas, A., Comastri, A., Ranalli, P., Vignali, C., Balestra, I., Gilli, R., and Cappelluti, N.: 2011, *Astron. Astroph.* **534**, A23.

Gilli, R., Salvati, M., and Hasinger, G.: 2001, *Astron. Astroph.* **366**, 407.

Gordon, K.D., Clayton, G.C., Misselt, K.A., Landolt, A.U., and Wolff, M.J.: 2003, *Astrophys. J.* **594**, 279.

Greene, J.E. and Ho, L.C.: 2005, *Astrophys. J.* **630**, 122.

Hao, H., Elvis, M., Bongiorno, A., Zamorani, G., Merloni, A., Kelly, B.C., Civano, F., Celotti, A., Ho, L.C., Jahnke, K., Comastri, A., Trump, J.R., Mainieri, V., Salvato, M., Brusa, M., Impey, C.D., Koekemoer, A.M., Lanzuisi, G., Vignali, C., Silverman, J.D., Urry, C.M., and Schawinski, K.: 2013, *Monthly Notices of the Royal Astronomical Society* **434**, 3104.

Hernández-García, L., Masegosa, J., González-Martín, O., and Márquez, I.: 2015, *Astron. Astroph.* **579**, A90.

Hopkins, P.F., Strauss, M.A., Hall, P.B., Richards, G.T., Cooper, A.S., Schneider, D.P., Vanden Berk, D.E., Jester, S., Brinkmann, J., and Szokoly, G.P.: 2004, *The Astronomical Journal* **128**, 1112.

Huang, X.-X., Wang, J.-X., Tan, Y., Yang, H., and Huang, Y.-F.: 2011, *Astrophys. J.* **734**, L16.

Jansen, F., Lumb, D., Altieri, B., Clavel, J., Ehle, M., Erd, C., Gabriel, C., Guainazzi, M., Gondoin, P., Much, R., Munoz, R., Santos, M., Schartel, N., Texier, D., and Vacanti, G.: 2001, *Astron. Astroph.* **365**, L1.

Jin, C., Ward, M., and Done, C.: 2012, *Monthly Notices of the Royal Astronomical Society* **422**, 3268.

Jones, D.H., Read, M.A., Saunders, W., Colless, M., Jarrett, T., Parker, Q.A., Fairall, A.P., Mauch, T., Sadler, E.M., Watson, F.G., Burton, D., Campbell, L.A., Cass, P., Croom, S.M., Dawe, J., Fiegert, K., Frankcombe, L., Hartley, M., Huchra, J., James, D., Kirby, E., Lahav, O., Lucey, J., Mamon, G.A., Moore, L., Peterson, B.A., Prior, S., Proust, D., Russell, K., Safouris, V., Wakamatsu, K.-I., Westra, E., and Williams, M.: 2009, *Monthly Notices of the Royal Astronomical Society* **399**, 683.

Kaspi, S., Smith, P.S., Netzer, H., Maoz, D., Jannuzi, B.T., and Giveon, U.: 2000, *Astrophys. J.* **533**, 631.

Koratkar, A. and Blaes, O.: 1999, *Publications of the Astronomical Society of the Pacific* **111**, 1.

Krumpe, M., Lamer, G., Markowitz, A., and Corral, A.: 2010, *Astrophys. J.* **725**, 2444.

López, S., D'Odorico, V., Ellison, S.L., Becker, G.D., Christensen, L., Cupani, G., Denney, K.D., Pâris, I., Worseck, G., Berg, T.A.M., Cristiani, S., Dessauges-Zavadsky, M., Haehnelt, M., Hamann, F., Hennawi, J., Iršič, V., Kim, T.-S., López, P., Lund Saust, R., Ménard, B., Perrotta, S., Prochaska, J.X., Sánchez-Ramírez, R., Vestergaard, M., Viel, M., and Wisotzki, L.: 2016, *Astron. Astroph.* **594**, A91.

LaMassa, S.M., Cales, S., Moran, E.C., Myers, A.D., Richards, G.T., Eracleous, M., Heckman, T.M., Gallo, L., and Urry, C.M.: 2015, *Astrophys. J.* **800**, 144.

Liedahl, D.A., Osterheld, A.L., and Goldstein, W.H.: 1995, *Astrophys. J.* **438**, L115.

Mainieri, V., Rosati, P., Tozzi, P., Bergeron, J., Gilli, R., Hasinger, G., Nonino, M., Lehmann, I., Alexander, D.M., Idzi, R., Koekemoer, A.M., Norman, C., Szokoly, G., and Zheng, W.: 2005, *Astron. Astroph.* **437**, 805.

Maiolino, R., Marconi, A., Salvati, M., Risaliti, G., Severgnini, P., Oliva, E., La Franca, F., and Vanzi, L.: 2001, *Astron. Astroph.* **365**, 28.

Malizia, A., Bassani, L., Bazzano, A., Bird, A.J., Masetti, N., Panessa, F., Stephen, J.B., and Ubertini, P.: 2012, *Monthly Notices of the Royal Astronomical Society* **426**, 1750.

Marchese, E., Della Ceca, R., Caccianiga, A., Severgnini, P., Corral, A., and Fanali, R.: 2012, *Astron. Astroph.* **539**, A48.

Markowitz, A.G., Krumpe, M., and Nikutta, R.: 2014, *Monthly Notices of the Royal Astronomical Society* **439**, 1403.

Masetti, N., Parisi, P., Jiménez-Bailón, E., Palazzi, E., Chavushyan, V., Bassani, L., Bazzano, A., Bird, A.J., Dean, A.J., Galaz, G., Landi, R., Malizia, A., Minniti, D., Morelli, L., Schiavone, F., Stephen, J.B., and Ubertini, P.: 2012, *Astron. Astroph.* **538**, A123.

Mason, K.O., Breeveld, A., Much, R., Carter, M., Cordova, F.A., Cropper, M.S., Fordham, J., Huckle, H., Ho, C., Kawakami, H., Kennea, J., Kennedy, T., Mittaz, J., Pandel, D., Priedhorsky, W.C., Sasseen, T., Shirey, R., Smith, P., and Vreux, J.-M.: 2001, *Astron. Astroph.* **365**, L36.

Mateos, S., Alonso-Herrero, A., Carrera, F.J., Blain, A., Watson, M.G., Barcons, X., Braito, V., Severgnini, P., Donley, J.L., and Stern, D.: 2012, *Monthly Notices of the Royal Astronomical Society* **426**, 3271.

Mateos, S., Barcons, X., Carrera, F.J., Ceballos, M.T., Caccianiga, A., Lamer, G., Maccacaro, T., Page, M.J., Schwope, A., and Watson, M.G.: 2005, *Astron. Astroph.* **433**, 855.

Mateos, S., Barcons, X., Carrera, F.J., Ceballos, M.T., Hasinger, G., Lehmann, I., Fabian, A.C., and Streblyanska, A.: 2005, *Astron. Astroph.* **444**, 79.

Mateos, S., Barcons, X., Carrera, F.J., Page, M.J., Ceballos, M.T., Hasinger, G., and Fabian, A.C.: 2007, *Astron. Astroph.* **473**, 105.

Mateos, S., Carrera, F.J., Alonso-Herrero, A., Rovilos, E., Hernán-Caballero, A., Barcons, X., Blain, A., Caccianiga, A., Della Ceca, R., and Severgnini, P.: 2015, *Monthly Notices of the Royal Astronomical Society* **449**, 1422.

Mateos, S., Carrera, F.J., Page, M.J., Watson, M.G., Corral, A., Tedds, J.A., Ebrero, J., Krumpe, M., Schwope, A., and Ceballos, M.T.: 2010, *Astron. Astroph.* **510**, A35.

Mateos, S., Saxton, R.D., Read, A.M., and Sembay, S.: 2009, *Astron. Astroph.* **496**, 879.

Mateus, A., Sodré, L., Cid Fernandes, R., Stasińska, G., Schoenell, W., and Gomes, J.M.: 2006, *Monthly Notices of the Royal Astronomical Society* **370**, 721.

Mehdipour, M., Branduardi-Raymont, G., and Page, M.J.: 2012, *Astron. Astroph.* **542**, A30.

Merloni, A., Bongiorno, A., Brusa, M., Iwasawa, K., Mainieri, V., Magnelli, B., Salvato, M., Berta, S., Cappelluti, N., Comastri, A., Fiore, F., Gilli, R., Koekemoer, A., Le Floc'h, E., Lusso, E., Lutz, D., Miyaji, T., Pozzi, F., Riguccini, L., Rosario, D.J., Silverman, J., Symeonidis, M., Treister, E., Vignali, C., and Zamorani, G.: 2014, *Monthly Notices of the Royal Astronomical Society* **437**, 3550.

Merritt, D. and Ferrarese, L.: 2001, *Monthly Notices of the Royal Astronomical Society* **320**, L30.

Mewe, R., Gronenschild, E.H.B.M., and van den Oord, G.H.J.: 1985, *Astronomy and Astrophysics Supplement Series* **62**, 197.

Mewe, R., Lemen, J.R., and van den Oord, G.H.J.: 1986, *Astronomy and Astrophysics Supplement Series* **65**, 511.

Miniutti, G., Sanfrutos, M., Beuchert, T., Agís-González, B., Longinotti, A.L., Piconcelli, E., Krongold, Y., Guainazzi, M., Bianchi, S., Matt, G., and Jiménez-Bailón, E.: 2014, *Monthly Notices of the Royal Astronomical Society* **437**, 1776.

Mortlock, D.J., Warren, S.J., Venemans, B.P., Patel, M., Hewett, P.C., McMahon, R.G., Simpson, C., Theuns, T., Gonzáles-Solares, E.A., Adamson, A., Dye, S., Hambly, N.C., Hirst, P., Irwin, M.J., Kuiper, E., Lawrence, A., and Röttgering, H.J.A.: 2011, *Nature* **474**, 616.

Netzer, H.: 2013, *The Physics and Evolution of Active Galactic Nuclei, by Hagai Netzer, Cambridge, UK: Cambridge University Press, 2013*.

Nisini, B., Giannini, T., Antoniucci, S., Alcalá, J.M., Bacciotti, F., and Podio, L.: 2016, *Astron. Astroph.* **595**, A76.

Noll, S. and Pierini, D.: 2005, *Astron. Astroph.* **444**, 137.

Page, M.J., Carrera, F.J., Stevens, J.A., Ebrero, J., and Blustin, A.J.: 2011, *Monthly Notices of the Royal Astronomical Society* **416**, 2792.

Panessa, F. and Bassani, L.: 2002, *Astron. Astroph.* **394**, 435.

Panessa, F., Bassani, L., Cappi, M., Dadina, M., Barcons, X., Carrera, F.J., Ho, L.C., and Iwasawa, K.: 2006, *Astron. Astroph.* **455**, 173.

Pappa, A., Georgantopoulos, I., Stewart, G.C., and Zezas, A.L.: 2001, *Monthly Notices of the Royal Astronomical Society* **326**, 995.

Parisi P.: 2011, *PhD thesis*, Univ. di Bologna

Park, D., Kelly, B.C., Woo, J.-H., and Treu, T.: 2012, *The Astrophysical Journal Supplement Series* **203**, 6.

Polletta, M., Tajer, M., Maraschi, L., Trinchieri, G., Lonsdale, C.J., Chiappetti, L., Andreon, S., Pierre, M., Le Fèvre, O., Zamorani, G., Maccagni, D., Garcet, O., Surdej, J., Franceschini, A., Alloin, D., Shupe, D.L., Surace, J.A., Fang, F., Rowan-Robinson, M., Smith, H.E., and Tresse, L.: 2007, *Astrophys. J.* **663**, 81.

Raimundo, S.I. and Fabian, A.C.: 2009, *Monthly Notices of the Royal Astronomical Society* **396**, 1217.

Risaliti, G. and Elvis, M.: 2004, *Supermassive Black Holes in the Distant Universe* **308**, 187.

Schmidt, K.B., Rix, H.-W., Shields, J.C., Knecht, M., Hogg, D.W., Maoz, D., and Bovy, J.: 2012, *Astrophys. J.* **744**, 147.

Schnorr-Müller, A., Davies, R.I., Korista, K.T., Burtscher, L., Rosario, D., Storchi-Bergmann, T., Contursi, A., Genzel, R., Graciá-Carpio, J., Hicks, E.K.S., Janssen, A., Koss, M., Lin, M.-Y., Lutz, D., Maciejewski, W., Müller-Sánchez, F., Orban de Xivry, G., Riffel, R., Riffel, R.A., Schartmann, M., Sternberg, A., Sturm, E., Tacconi, L., Veilleux, S., and Ulrich, O.A.: 2016, *Monthly Notices of the Royal Astronomical Society* **462**, 3570.

Scott, A.E., Stewart, G.C., and Mateos, S.: 2012, *Monthly Notices of the Royal Astronomical Society* **423**, 2633.

Setti, G. and Woltjer, L.: 1989, *Astron. Astroph.* **224**, L21.

Severgnini, P., Caccianiga, A., Braito, V., Della Ceca, R., Maccacaro, T., Wolter, A., Sekiguchi, K., Sasaki, T., Yoshida, M., Akiyama, M., Watson, M.G., Barcons, X., Carrera, F.J., Pietsch, W., and Webb, N.A.: 2003, *Astron. Astroph.* **406**, 483.

Shen, Y.: 2016, *Astrophys. J.* **817**, 55.

Singh, K.P.: 2013, *Bulletin of the Astronomical Society of India* **41**, 137.

Spiniello, C., Trager, S.C., Koopmans, L.V.E., and Chen, Y.P.: 2012, *Astrophys. J.* **753**, L32.

Steinhardt, C.L., Schramm, M., Silverman, J.D., Alexandroff, R., Capak, P., Civano, F., Elvis, M., Masters, D., Mobasher, B., Pattarakijwanich, P., and Strauss, M.A.: 2012, *Astrophys. J.* **759**, 24.

Stern, D.: 2015, *Astrophys. J.* **807**, 129.

Stern, J. and Laor, A.: 2012, *Monthly Notices of the Royal Astronomical Society* **426**, 2703.

Strüder, L., Briel, U., Dennerl, K., Hartmann, R., Kendziorra, E., Meidinger, N., Pfeffermann, E., Reppin, C., Aschenbach, B., Bornemann, W., Bräuninger, H., Burkert, W., Elender, M., Freyberg, M., Haberl, F., Hartner, G., Heuschmann, F., Hippmann, H., Kastelic, E., Kemmer, S., Kettenring, G., Kink, W., Krause, N., Müller, S., Oppitz, A., Pietsch, W., Popp, M., Predehl, P., Read, A., Stephan, K.H., Stötter, D., Trümper, J., Holl, P., Kemmer, J., Soltau, H., Stötter, R., Weber, U., Weichert, U., von Zanthier, C., Carathanassis, D., Lutz, G., Richter, R.H., Solc, P., Böttcher, H., Kuster, M., Staubert, R., Abbey, A., Holland, A., Turner, M., Balasini, M., Bignami, G.F., La Palombara, N., Villa, G., Buttler, W., Gianini, F., Lainé, R., Lumb, D., and Dhez, P.: 2001, *Astron. Astroph.* **365**, L18.

Sulentic, J.W., Marziani, P., and Dultzin-Hacyan, D.: 2000, *Annual Review of Astronomy and Astrophysics* **38**, 521.

Taylor, E.N., Franx, M., Brinchmann, J., van der Wel, A., and van Dokkum, P.G.: 2010, *Astrophys. J.* **722**, 1.

Tozzi, P., Gilli, R., Mainieri, V., Norman, C., Risaliti, G., Rosati, P., Bergeron, J., Borgani, S., Giacconi, R., Hasinger, G., Nonino, M., Streblyanska, A., Szokoly, G., Wang, J.X., and Zheng, W.: 2006, *Astron. Astroph.* **451**, 457.

Trippe, M.L., Crenshaw, D.M., Deo, R.P., Dietrich, M., Kraemer, S.B., Rafter, S.E., and Turner, T.J.: 2010, *Astrophys. J.* **725**, 1749.

Trippe, S.: 2015, *Journal of Korean Astronomical Society* **48**, 203.

Turner, M.J.L., Abbey, A., Arnaud, M., Balasini, M., Barbera, M., Belsole, E., Bennie, P.J., Bernard, J.P., Bignami, G.F., Boer, M., Briel, U., Butler, I., Cara, C., Chabaud, C., Cole, R., Collura, A., Conte, M., Cros, A., Denby, M., Dhez, P., Di Coco, G., Dowson, J., Ferrando, P., Ghizzardi, S., Gianotti, F., Goodall, C.V., Gretton, L., Griffiths, R.G., Hainaut, O., Hochedez, J.F., Holland, A.D., Jourdain, E., Kendziorra, E., Lagostina, A., Laine, R., La Palombara, N., Lortholary, M., Lumb, D., Marty, P., Molendi, S., Pigot, C., Poindron, E., Pounds, K.A., Reeves, J.N., Reppin, C., Rothenflug, R., Salvetat, P., Sauvageot, J.L., Schmitt, D., Sembay, S., Short, A.D.T., Spragg, J., Stephen, J., Strüder, L., Tiengo, A., Trifoglio, M., Trümper, J., Vercellone, S., Vigroux, L., Villa, G., Ward, M.J., Whitehead, S., and Zonca, E.: 2001, *Astron. Astroph.* **365**, L27.

Turner, T.J. and Miller, L.: 2009, *Astronomy and Astrophysics Review* **17**, 47.

Ulrich, M.-H., Maraschi, L., and Urry, C.M.: 1997, *Annual Review of Astronomy and Astrophysics* **35**, 445.

Urry, C.M. and Padovani, P.: 1995, *Publications of the Astronomical Society of the Pacific* **107**, 803.

van Dokkum, P.G.: 2001, *Publications of the Astronomical Society of the Pacific* **113**, 1420.

Vasudevan, R.V., Mushotzky, R.F., Winter, L.M., and Fabian, A.C.: 2009, *Monthly Notices of the Royal Astronomical Society* **399**, 1553.

Vernet, J., Dekker, H., D'Odorico, S., Kaper, L., Kjaergaard, P., Hammer, F., Randich, S., Zerbi, F., Groot, P.J., Hjorth, J., Guinouard, I., Navarro, R., Adolfse, T., Albers, P.W., Amans, J.-P., Andersen, J.J., Andersen, M.I., Binetruy, P., Bristow, P., Castillo, R., Chemla, F., Christensen, L., Conconi, P., Conzelmann, R., Dam, J., de Caprio, V., de Ugarte Postigo, A., Delabre, B., di Marcantonio, P., Downing, M., Elswijk, E., Finger, G., Fischer, G., Flores, H., François, P., Goldoni, P., Guglielmi, L., Haigron, R., Hanenburg, H., Hendriks, I., Horrobin, M., Horville, D., Jessen, N.C., Kerber, F., Kern, L., Kiekebusch, M., Kleszcz, P., Klougart, J., Kragt, J., Larsen, H.H., Lizon, J.-L., Lucuix, C., Mainieri, V., Manuputy, R., Martayan, C., Mason, E., Mazzoleni, R., Michaelsen, N., Modigliani, A., Moehler, S., Møller, P., Norup Sørensen, A., Nørregaard, P., Péroux, C., Patat, F., Pena, E., Pragt, J., Reinero, C., Rigal, F., Riva, M., Roelfsema, R., Royer, F., Sacco, G., Santin, P., Schoenmaker, T., Spano, P., Sweers, E., Ter Horst, R., Tintori, M., Tromp, N., van Dael, P., van der Vliet, H., Venema, L., Vidali, M., Vinther, J., Vola, P., Winters, R., Wistisen, D., Wulterkens, G., and Zacchei, A.: 2011, *Astron. Astroph.* **536**, A105.

Véron-Cetty, M.P. and Véron, P.: 2000, *Astronomy and Astrophysics Review* **10**, 81.

Véron-Cetty, M.-P., and Véron, P.: 2006, *Astron. Astroph.* **455**, 773.

Vitale, M., Mignoli, M., Cimatti, A., Lilly, S.J., Carollo, C.M., Contini, T., Kneib, J.-P., Le Fevre, O., Mainieri, V., Renzini, A., Scodeggio, M., Zamorani, G., Bardelli, S., Barnes, L., Bolzonella, M., Bongiorno, A., Bordoloi, R., Bschorr, T.J., Cappi, A., Caputi, K., Coppa, G., Cucciati, O., de la Torre, S., de Ravel, L., Franzetti, P., Garilli, B., Iovino, A., Kampczyk, P., Knobel, C., Koekemoer, A.M., Kovač, K., Lamareille, F., Le Borgne, J.-F., Le Brun, V., López-Sanjuan, C., Maier, C., McCracken, H.J., Moresco, M., Nair, P., Oesch, P.A., Pello, R., Peng, Y., Pérez Montero, E., Pozzetti, L., Presotto, V., Silverman, J., Tanaka, M., Tasca, L., Tresse, L., Vergani, D., Welikala, N., and Zucca, E.: 2013, *Astron. Astroph.* **556**, A11.

Watson, M.G., Schröder, A.C., Fyfe, D., Page, C.G., Lamer, G., Mateos, S., Pye, J., Sakano, M., Rosen, S., Ballet, J., Barcons, X., Barret, D., Boller, T., Brunner, H., Brusa, M., Caccianiga, A., Carrera, F.J., Ceballos, M., Della Ceca, R., Denby, M., Denkinson, G., Dupuy, S., Farrell, S., Fraschetti, F., Freyberg, M.J., Guillout, P., Hambaryan, V., Maccacaro, T., Mathiesen, B., McMahon, R., Michel, L., Motch, C., Osborne, J.P., Page, M., Pakull, M.W., Pietsch, W., Saxton, R., Schwope, A., Severgnini, P., Simpson, M., Sironi, G., Stewart, G., Stewart, I.M., Stobbart, A.-M., Tedds, J., Warwick, R., Webb, N., West, R., Worrall, D., and Yuan, W.: 2009, *Astron. Astroph.* **493**, 339.

Wilkes, B.J., Schmidt, G.D., Cutri, R.M., Ghosh, H., Hines, D.C., Nelson, B., and Smith, P.S.: 2002, *Astrophys. J.* **564**, L65.

Wilman, R.J. and Fabian, A.C.: 1999, *Monthly Notices of the Royal Astronomical Society* **309**, 862.

Wright, E.L., Eisenhardt, P.R.M., Mainzer, A.K., Ressler, M.E., Cutri, R.M., Jarrett, T., Kirkpatrick, J.D., Padgett, D., McMillan, R.S., Skrutskie, M., Stanford, S.A., Cohen, M., Walker, R.G., Mather, J.C., Leisawitz, D., Gautier, T.N., III, McLean, I., Benford, D., Lonsdale, C.J., Blain, A., Mendez, B., Irace, W.R., Duval, V., Liu, F., Royer, D., Heinrichsen, I., Howard, J., Shannon, M., Kendall, M., Walsh, A.L., Larsen, M., Cardon, J.G., Schick, S., Schwalm, M., Abid, M., Fabinsky, B., Naes, L., and Tsai, C.-W.: 2010, *The Astronomical Journal* **140**, 1868-1881.

Young, M., Elvis, M., and Risaliti, G.: 2008, *Astrophys. J.* **688**, 128-147.

Padovani, P., Alexander, D.M., Assef, R.J., De Marco, B., Giommi, P., Hickox, R.C., Richards, G.T., Smolčić, V., Hatziminaoglou, E., Mainieri, V., and Salvato, M.: 2017, *Astronomy and Astrophysics Review* **25**, 2.

Gilli, R., Comastri, A., and Hasinger, G.: 2007, *Astron. Astroph.* **463**, 79.

Seyfert, C.K.: 1943, *Astrophys. J.* **97**, 28.

Kant, I.: 1755. *Allgemeine Naturgeschichte und Theorie des Himmels* , Part I, J.F. Peterson, Königsberg and Leipzig.

Hubble, E.P.: 1929, *Astrophys. J.* **69**.

Hönig, S.F., Watson, D., Kishimoto, M., Gandhi, P., Goad, M., Horne, K., Shankar, F., Banerji, M., Boulderstone, B., Jarvis, M., Smith, M., and Sullivan, M.: 2017, *Monthly Notices of the Royal Astronomical Society* **464**, 1693.

Magorrian, J., Tremaine, S., Richstone, D., Bender, R., Bower, G., Dressler, A., Faber, S.M., Gebhardt, K., Green, R., Grillmair, C., Kormendy, J., and Lauer, T.: 1998, *The Astronomical Journal* **115**, 2285.

Kormendy, J. and Ho, L.C.: 2013, *Annual Review of Astronomy and Astrophysics* **51**, 511.

Fabian, A.C.: 2012, *Annual Review of Astronomy and Astrophysics* **50**, 455.

Maiolino, R., Marconi, A., and Oliva, E.: 2001, *Astron. Astroph.* **365**, 37.

Netzer, H.: 1990 *Active Galactic Nuclei*, AGN Emission Lines, eds. R.D. Blandford, H. Netzer and L. Woltjer.

Whittle, M.: 1992, *The Astrophysical Journal Supplement Series* **79**, 49.

Laing R. A., Jenkins C. R., Wall J. V., Unger S. W.: 1994, *Spectrophotometry of a Complete Sample of 3CR Radio Sources: Implications for Unified Models*. The Physics of Active Galaxies 54: 201

Weingartner, J.C. and Draine, B.T.: 2001, *Astrophys. J.* **548**, 296.

Fanaroff, B.L. and Riley, J.M.: 1974, *Monthly Notices of the Royal Astronomical Society* **167**, 31P.

Granato, G.L., Danese, L., and Franceschini, A.: 1997, *Astrophys. J.* **486**, 147.

Osterbrock, D.E.: 1991, *Reports on Progress in Physics* **54**, 579.

Padovani, P.: 2016, *Astronomy and Astrophysics Review* **24**, 13.

Giommi, P., Padovani, P., Polenta, G., Turriziani, S., D'Elia, V., and Piranomonte, S.: 2012, *Monthly Notices of the Royal Astronomical Society* **420**, 2899.

Weymann, R.J., Carswell, R.F., and Smith, M.G.: 1981, *Annual Review of Astronomy and Astrophysics* **19**, 41.

Ghisellini, G.: 2010, *American Institute of Physics Conference Series* **1242**, 43.

O'Dea, C.P., Baum, S.A., and Stanghellini, C.: 1991, *Astrophys. J.* **380**, 66.

Padovani, P. and Giommi, P.: 1995, *Astrophys. J.* **444**, 567.

Heckman, T.M. and Best, P.N.: 2014, *Annual Review of Astronomy and Astrophysics* **52**, 589.

Ho, L.C.: 2008, *Annual Review of Astronomy and Astrophysics* **46**, 475.

Osterbrock, D.E. and Pogge, R.W.: 1985, *Astrophys. J.* **297**, 166.

Sulentic, J.W., Marziani, P., Zamanov, R., Bachev, R., Calvani, M., and Dultzin-Hacyan, D.: 2002, *Astrophys. J.* **566**, L71.

Osterbrock, D.E.: 1981, *Astrophys. J.* **249**, 462.

Osterbrock, D.E.: 1989, *Research supported by the University of California, John Simon Guggenheim Memorial Foundation, University of Minnesota, et al. Mill Valley, CA, University Science Books, 1989, 422 p.*.

Ueda, Y., Akiyama, M., Ohta, K., and Miyaji, T.: 2003, *Astrophys. J.* **598**, 886.

Beckmann, V. and Shrader, C.: 2012, *Proceedings of "An INTEGRAL view of the high-energy sky (the first 10 years)" - 9th INTEGRAL Workshop and celebration of the 10th anniversary of the launch (INTEGRAL 2012). 15-19 October 2012. Bibliotheque Nationale de France, Paris, France. Published online at ¡A href="http://pos.sissa.it/cgi-bin/reader/conf.cgi?confid=176"¿http://pos.sissa.it/cgi-bin/reader/conf.cgi?confid=176¡/A¿, id.69*, 69.

Goodrich, R.W., Veilleux, S., and Hill, G.J.: 1994, *Astrophys. J.* **422**, 521.

Antonucci, R.R.J. and Miller, J.S.: 1985, *Astrophys. J.* **297**, 621.

Miller, J.S. and Goodrich, R.W.: 1990, *Astrophys. J.* **355**, 456.

Tran, H.D., Miller, J.S., and Kay, L.E.: 1992, *Astrophys. J.* **397**, 452.